TECHNICAL UNIVERSITY OF LIBEREC
Faculty of Mechatronics, Informatics and
Interdisciplinary Studies
Institute of Mechatronics and Computer Engineering

CONTROL OF STATIC AND DYNAMIC MECHANICAL RESPONSE OF PIEZOELECTRIC COMPOSITE SHELLS: APPLICATIONS TO ACOUSTICS AND ADAPTIVE OPTICS

by

KATEŘINA NOVÁKOVÁ

DISSERTATION THESIS REVIEW

PhD programme: Science Engineering

Liberec 2013

Thesis Supervisor:
doc. Ing. Pavel Mokrý, Ph.D.
Institute of Mechatronics and Computer Engineering
Faculty of Mechatronics, Informatics and Interdisciplinary Studies
Technical University of Liberec
Studentská 1402/2
CZ46117 Liberec I
Czech Republic

Abstract

This dissertation thesis (Thesis) deals with the study of possibilities to actively control the static and dynamic mechanical response of planar structures by means of attached piezoelectric actuators. The considered planar structures have a form of flat or curved piezoelectric composite shells. It will be shown that such piezoelectric composite shells can provide efficient and rather simple mechatronic systems that can be profitably used in applications to acoustics and adaptive optics.

In acoustics, the piezoelectric composite shells represent an interface between two acoustic media. Existence of such an interface affects tremendously the sound wave propagation through it. It is known that, when the incident sound wave hits the shell, it makes the shell vibrate. The shell vibration causes that a part of the incident sound wave is reflected and a part is transmitted. It will be shown that by controlling the amplitude of the shell vibration, it is possible to control the amplitudes of the reflected and transmitted waves. Such a principle offers a simple approach for a construction of noise control systems.

A physical parameter, which expresses the sound shielding efficiency of noise control systems, is called the acoustic transmission loss. Therefore, a considerable part of the Thesis is devoted to the analytical calculation or numerical computation of the acoustic transmission loss of several systems with piezoelectric composite shells. It will be demonstrated that by connecting the piezoelectric composite shell to an active electric (shunt) circuit, it is possible to control the acoustic transmission loss of the shell. Such an effect can be easily explained by considering the effective elastic properties of the piezoelectric composite shell shunted by an active electric circuit. It will be shown that acoustic transmission loss of the shell is increased, when the effective Young's modulus or the bending stiffness coefficient of the shell are increased. Such an increase in the elastic parameters of the piezoelectric composite shell can be achieved by the proper construction and adjustment of the shunt circuit connected to the piezoelectric actuators in the piezoelectric composite shell.

The numerical computation of the acoustic transmission loss can be divided into two steps. In the first step, it is necessary to investigate the effect of the shunt circuit on the elastic properties of the piezoelectric actuator, which is attached to the glass shell. In the second step, the effect of the elastic parameters of the piezoelectric actuator on the acoustic transmission loss of the piezoelectric composite shell is analyzed. In the presented work, the utilization of so called the Macro-Fiber-Composite (MFC) actuator is considered, since it is suitable for easy attachment to flat or curved glass shells. In accord with the aforementioned approach and due to geometrical complexity of the MFC actuator, the numerical model of the MFC actu-

ator based on the finite element method (FEM) is developed. The FEM model of the MFC actuator has been used for the numerical computation of effective elastic parameters, macroscopic piezoelectric constants, and the capacitance per unit area of the MFC actuator. The effect of the shunt electric circuit on the macroscopic properties of the MFC actuator is analyzed and the method for the determination of optimal shunt circuit parameters that yield maximum values of effective Young's moduli is presented. Then, a detailed analysis of the particular geometry of the glass plate and the arrangement of MFC actuators on the glass plate is performed using a FEM model. Finally, the functionality of the approach and the developed numerical models are verified using acoustic experiments.

In the last part of the Thesis, an application of electronic control of the shape of planar structures in adaptive optics is introduced. An optimization of several geometric parameters of a deformable mirror that consists of a nickel reflective layer deposited on top of a thin piezoelectric PZT disk to get the maximum actuator stroke is presented using the FEM simulations of the layered composite structure.

Keywords:

Acoustics, Adaptive optics, Planar structure, Glass window, Macro Fiber Composite piezoelectric actuator, Noise transmission control, Elastic properties control, Active circuit, Negative capacitor, FEM simulations.

Contents

Chapter 1

Introduction

1.1 Motivation

It is known that the vibration of large planar structures (e.g. airplane wings, large windows, glass facades or various flexible panels) results in a serious material fatigue, weakening joints, increase in skin friction, or an unpleasant noise produced directly by vibrating structures. All these bothering effects represent a stimulation for a research of sophisticated methods for the suppression of vibration and noise transmission through large planar structures. Realization of such methods has become a big contemporary challenge for scientists and researchers in the fields of mechanical engineering and acoustics. Therefore, the objective of the dissertation thesis (Thesis) is to develop methods for the noise suppression through planar structures.

Nowadays, the noise suppression became an environmental problem because people in cities are exposed to many harmful influences on their health caused by the unpleasant noise. In the quest of prevention the hearing illnesses, it seems to be reasonable to suppress the noise at places where people live and work. It is a quite hard task, because the intensity of the noise in cities is becoming permanently bigger and passive noise suppression methods are not sufficient, especially in the low frequency range (up to 1 kHz). On the other hand, active noise suppression methods work well in a low frequency range (up to 1 kHz) but they require complicated control algorithms and very fast electronics.

The new approach of modern noise suppression methods should be based on the sound transmission control. Besides other things, the most important requirements for these methods is the noise suppression system effectiveness in wide frequency range, especially between 2 and 5 kHz, where the human hearing is inclined to be easily harmed [1, 2].

1.2 Problem Statement

The key objective of the Thesis is the study of possibilities of a precise active control of static and dynamic mechanical response of planar structures. Two possible areas of applications, where the controlled planar structures can be used, are, first, structural acoustics, where the planar structures (windows or glazed facades) represent major paths of noise transmission into a building interior. They can be actively controlled by means of their acoustic impedance. Second application area, where the tuned planar structures can be used, is adaptive optics, where the most commonly used planar structures as wavefront correctors are large diameter deformable mirrors, which require a fast response time and a strong actuation stroke. In order to achieve large deflections over the surface of the planar structures, devices based on piezoelectric layer composite structures actively controlled by the electric field are designed. The basic principles of the vibrational control of planar structures are explained and demonstrated on a simple example of a sound transmission through a glass plate window.

Today, there exist several passive noise control techniques, which are based on the application of elements, such as massive walls, rubber layers, porous materials, etc. Such methods are relatively cheap and efficient in high frequency range. However, it is clear that they can be hardly applicable to large glass windows or facades. At the same time, there exist conventional active noise control techniques. These methods are efficient in the low frequency range, but it is difficult to find their implementation that would be both efficient in a broad frequency range and financially acceptable. The third category of noise suppression methods is based on the semi-active control approach, which profitably balances the advantages of both passive and active approaches: a high efficiency, a simple technical implementation, a minimal weight and size, a low cost, and small external power supply. This technique is in literature commonly referred to as a piezoelectric shunt damping (PSD). It uses the piezoelectric actuator mechanically attached to the structure and electrically shunted by passive or active electrical networks. This promising approach is characterized by utilization of piezoelectric materials in an alternative way based on a simultaneous sensing and actuation performed by a single either monolithic or composite piezoelectric actuator, which is connected to a one-port shunt circuit.

1.3 Contributions of the Thesis

A relevance of the problem solved in the Thesis can be measured in terms of approach originality, global social benefits, and potential commercial profits. The approach presented in the Thesis offers a promising method for the control of the static and dynamic deformations of planar structures. In Thesis, there is analyzed and verified the functionality of the method on a system for the suppression of noise transmission through the glass windows using the active control of the acoustic impedance of the glass plate with attached piezoelectric actuators shunted by an active electric circuit. The advantages of this method stem from its generality and simplicity, offering an efficient tool for the control of the noise transmission through glass windows, especially in the low-frequency range, in which passive methods are inefficient.

The social benefits can be found in the contribution to reduction of the urban and traffic noisiness in buildings and consequently to living and working comfort increase.

From the commercial point of view, the noise control method based on the piezoelectric shunt damping can bring an affordable higher comfort of services such as transport or accommodation thanks to an inexpensive and effective noise reduction. Potential success of the applied technology would lead to a higher competitiveness of the final services and products on the world markets thanks to its low costs and the efficiency in a wide range of frequencies.

1.4 Structure of the Thesis

The Thesis is organized into 6 chapters as follows:

- *Chapter 1. Introduction* describes the motivation behind the work efforts together with the goals. There is also a list of contributions of this Thesis and briefly indicated the outline.

- *Chapter 2. Background and State-of-the-Art* introduces the reader to the necessary theoretical background and surveys the current state-of-the-art. The theoretical background presents basics about smart materials and puts emphasis on piezoelectric materials. Also, there is defined the acoustic transmission loss (TL) as the main physical quantity evaluating the sound shielding efficiency of the interface between two acoustic media. The literature review is focused on the noise transmission control using smart, especially piezoelectric materials.

- *Chapter 3. Theoretical modelling of the acoustic impedance of a curved glass shell and the principles of active elasticity control method* determines the most important features of the noise transmission through planar structures using the approximative analytical model of the specific acoustic impedance of the curved shell. It is demonstrated that by an active piezoelectric layer attached to the planar structure it is possible to control the effective elastic properties of the whole structure. Also, the basic theoretical aspects of active control of effective elastic properties of piezoelectric materials are explained.

- *Chapter 4. Active elasticity control of macro fiber composite actuator* introduces a macro fiber composite (MFC) actuator such as active piezoelectric layer which could be attached to a vibrating structure without cracking. The static and dynamic response of the MFC actuator is analyzed in detail using finite element method (FEM) simulations. Computation of its effective material properties and demonstration of tuning its effective elastic constants by means of a shunt electric circuit is presented in this Chapter. Particularly, it is solved the effect of the shunt circuit with a negative capacitance (NC) on the effective elastic properties of the MFC actuator.

- *Chapter 5. Glass plate noise transmission suppression by means of distributed MFC actuators shunted by the negative capacitance circuit*: The objective of the study presented in this Chapter is to analyze the most efficient ways for suppression of noise transmission through the glass plates using active elasticity control of attached piezoelectric MFC actuators. A detailed analysis of the FEM model implementation of the particular arrangement of MFC actuators on the glass plate is performed. A simple experimental setup for the approximative measurements of the acoustic transmission loss is described. Results of the FEM model simulations and their comparison with experimental data are presented.

- *Chapter 6. Application of the active shape control of the planar structure to adaptive optics* introduces the deformable mirrors as the most commonly used wavefront correctors in adaptive optics systems. An optimization of several geometric parameters of a deformable mirror that consists of a nickel reflective layer deposited on top of a thin piezoelectric PZT disk to get the maximum actuator stroke is presented using the FEM simulations of the layered composite structure.

- *Conclusions*: Summarizes the results of the research presented in the Thesis.

Chapter 2

Theoretical Background

This Chapter introduces the reader to the necessary theoretical background about piezoelectric materials. The mathematical description of the piezoelectric effect is introduced to an extent, which is necessary for understanding its applications to the noise control through planar structures presented in the Thesis. For more extensive information, the reader should consult literature dedicated to the field of piezoelectrics such as in [3] or [4]. Useful information can be found in the IEEE Standard on Piezoelectricity [5] and more popular reading with recent aspects of the field of piezoelectricity is published in [6].

In addition, the acoustic transmission loss (TL) as the main physical quantity that measures/expresses the sound shielding efficiency of the device will be introduced.

2.1 Piezoelectric materials

In the wide range of the group of so called *smart materials* the most commonly used electro - mechanical transducers are piezoelectric materials. They provide excellent actuation and sensing capabilities, which are very valuable, e.g., in structural vibration control applications.

Nowadays, piezoelectric transducers are of many types and available in many forms and shapes. Piezoelectric effect can be observed in various types of materials, such as single crystals (e.g. quartz, barium titanate, lithium niobate), ceramics (e.g. lead zirconate titanate (PZT)), thin epitaxial films (e.g. the layer of PZT of the thickness of the order of μm and mm), polymers (e.g. polyvinylidene fluoride (PVDF)), or various composite structures. For more detailed overview of these types of materials, the reader should take a look at the recent publication edited by Safari and Akdogan ([7]).

Piezoelectric ceramics is the most commonly used piezoelectric mate-

rial. Currently, the search for new technologies has resulted in advanced composites from PZT that are light in weight, shape flexible and high in strength and stiffness compared to more conventional material systems. The possibility to use these piezoelectric composite structures contributed to being of the motivation of the Thesis.

The relationship between mechanic and electric energy conversion can be described by basic electromechanical equations. Their interpretation of the piezoelectric state equations is based on the IEEE standard for piezoelectricity [5]. The mathematical description of the electromechanical interaction in piezoelectrics combines the piezoelectric effect, the electrical behavior of the material and the Hooke's law. These physical phenomena are coupled in the set of two summation equations, where the first one describes the direct piezoelectric effect and the second one describes the inverse piezoelectric effect. In the constitutive equations, it is assumed that the total strain in the transducer is the sum of mechanical strain induced by the mechanical stress and the induced strain caused by the applied electric voltage. Assuming the simplified situation, i.e. the thermodynamic state when the temperature Θ or the entropy σ are constant values, the basic relationships between the electrical and elastic properties in piezoelectric materials are expressed in Einstein notation (introduced by Albert Einstein in 1916 [8]) as follows:

$$\begin{aligned} T_{ij} &= c^E_{ijkl} S_{kl} - e_{ijk} E_k \\ D_i &= e_{ikl} S_{kl} + \epsilon^S_{ij} E_j \end{aligned} \tag{2.1a}$$

$$\begin{aligned} T_{ij} &= c^D_{ijkl} S_{kl} - h_{ijk} D_k \\ E_i &= -h_{ikl} S_{kl} + \beta^S_{ij} D_j \end{aligned} \tag{2.1b}$$

$$\begin{aligned} S_{ij} &= s^E_{ijkl} T_{kl} + d_{ijk} E_k \\ D_i &= d_{ikl} T_{kl} + \epsilon^T_{ij} E_j \end{aligned} \tag{2.1c}$$

$$\begin{aligned} S_{ij} &= s^D_{ijkl} T_{kl} + g_{ijk} D_k \\ E_i &= -g_{ikl} T_{kl} + \beta^T_{ij} D_j, \end{aligned} \tag{2.1d}$$

where i, j, k, l are indexes of the material properties and state variables tensors from 1 to 3. Symbols T_{ij}, S_{ij}, E_i and D_i refer to the state variables, i.e. the components of the mechanical stress tensor, mechanical strain tensor, electric field vector and dielectric displacement vector, respectively.

Symbols ϵ_{ij} and β_{ij} stand for the electrical permittivity and impermittivity tensor components. The permittivity determines the charge per unit

area in the i-axis due to an electric field applied in the j-axis. In this notation, it is assumed that the permittivity is a product of the relative permittivity ϵ_r and the vacuum permittivity (permittivity of free space) $\epsilon_0 \approx 8.854187817\ \mathrm{F{\cdot}m^{-1}}$. Furthermore, the superscript T or S refers to the permittivity ϵ^T or ϵ^S, when the material is under constant mechanical stress or strain influence.

Elastic material parameters are expressed by the tensors of elastic compliance coefficients s_{ijkl} and elastic stiffness coefficients c_{ijkl}. Elastic compliance is the ratio of the strain the in ij-direction to the stress in the kl-direction, given that there is no change of stress along the other two directions. Elastic stiffness tensor is the inverse matrix to the elastic compliance tensor. A superscript E is used to state that the elastic compliance s^E_{ijkl} is measured with the electrodes short-circuited. Similarly, the superscript D in s^D_{ijkl} denotes that the measurements were taken when the electrodes were left open-circuited.

And last, d_{ikl}, e_{ikl}, g_{ijk} and h_{ijk} are the symbols indicating the piezoelectric coefficients which differ in terms which state variables are involved in the energy transformation. There are 4 possible combinations of the state variables during the mechanical into the electrical energy and vice versa transformation, so the four piezoelectric coefficients exist. E.g. the piezoelectric coefficient d_{ijk} is the ratio of the induced strain S_{ij} in jk-direction to the electric field E_i applied along the i-axis, when all external stresses are held constant.

One of the most important factors, which denote the efficiency of the conversion of the electrical energy into the mechanical energy, or vice versa, is the electromechanical coupling factor k_{ijk}. In Voigt notation it can be simplified to the $k_{i\lambda}$, where λ index ranges from 1 to 6. The indexes indicate that the stress, or strain are applied or developed in the direction λ, and the electrodes of the piezoelectric element are perpendicular to the i-axis. The electromechanical coupling factor measures the square root of converted over input energy fraction [9].

Lets assume that electric field E_j is applied to a piezoelectric material. Taking into account the relation of the electrical energy per unit volume,

$$U_e = \frac{1}{2} D_i E_j = \frac{1}{2} \epsilon_{ij} E_j^2, \tag{2.2}$$

and the stored mechanical mechanical energy per unit volume under zero external stress,

$$U_m = \frac{1}{2} S_\lambda T_\mu = \frac{1}{2} \frac{S_\lambda^2}{s_{\lambda\mu}}, \tag{2.3}$$

the relationship for the electromechanical factor can be expressed in terms

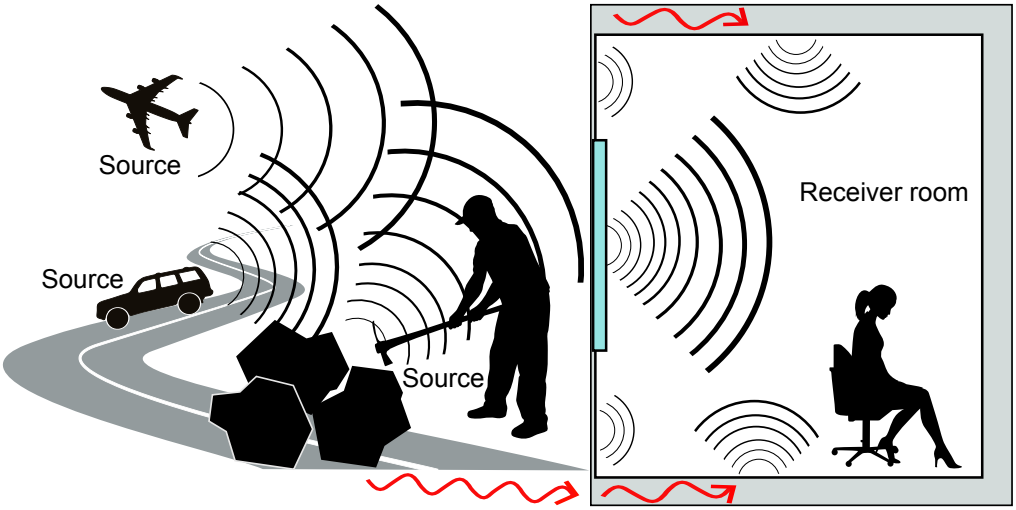

Figure 2.1: Noise transmission paths between an environment and adjacent building/room. Here, the major noise transmission path to buildings is the window.

of material constants. In particular,

$$k_{i\lambda}^2 = \frac{U_m}{U_e} = \frac{d_{i\lambda}^2}{s_{\lambda\mu}\epsilon_{ij}^T}, \tag{2.4}$$

where for the induced strain in piezoelectric materials holds the relationship $S_\lambda = d_{j\lambda}Ej$. As it could be seen from the Eq. (2.4), the electromechanical coupling factor is a unitless number from 0 to 1.

The electromechanical coupling factor is a very important parameter, because it characterizes the performance efficiency of the piezoelectric transducer. It has also a direct impact on the device bandwidth. For many applications, such as noise or vibration control, the electromechanical coupling factor is a crucial parameter for the design of the shunt electronics.

2.2 Acoustic transmission loss

Many environmental noise sources cause vibrations of various structures by the incident acoustic pressure waves. Due to their physical nature, structure vibrations are accompanied with the flow of mechanical or acoustic energy. In Fig. 2.1, it is pictured how the noise can transmit into buildings. The vibrations spread to adjacent structures, whose vibrations can cause the structure-born noise. So, the vibrating structures can be considered as secondary noise sources. If it is succeeded the suppression of this secondary structure-born noise, one does not have to pay attention to the sound fields generated by primary noise sources from outside.

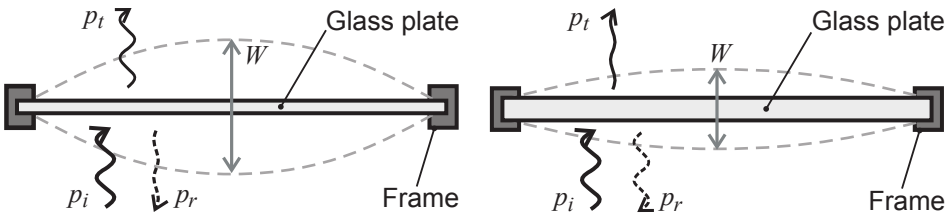

Figure 2.2: (a) Scheme of the considered sound transmission system, which consists of the glass plate fixed in a rigid frame at its edges. (b) Scheme of the noise suppression principle: When the vibration amplitude normal to the surface of the glass plate is reduced (e.g. due to being thicker), the greater part of the incident sound wave energy is reflected than transmitted.

As mentioned in the Introduction, large planar structures (flexible plates or panels), which vibrate, represent a substantial secondary noise source. The reason for this is that they usually do not represent an effective noise barrier due to their low flexural rigidity. Therefore, it is very easy to make them vibrate by the action of incident acoustic waves. Then, non-negligible part of the wave is transmitted through the window to the building interior.

In order to quantify the acoustic waves propagation in an acoustic medium and the reflection of the sound at the interface of two different media, we define a physical property called the acoustic impedance z (in $\mathrm{Pa{\cdot}s{\cdot}m^{-3}}$). It is a frequency-dependent parameter defined as an acoustic sound pressure p divided by particle velocity v and a surface area S, through which an acoustic wave propagates:

$$z = \frac{p}{vS}. \tag{2.5}$$

When dealing with planar structures, it is often convenient to express the acoustic impedance per unit area of the structure, which is made using a physical property called specific acoustic impedance Z (in $\mathrm{Pa{\cdot}s{\cdot}m^{-1}}$),

$$Z = \frac{p}{v}. \tag{2.6}$$

If a sound wave propagates through a medium, its wave motion is characterized by a physical property called characteristic acoustic impedance (in $\mathrm{Pa{\cdot}s{\cdot}m^{-1}}$):

$$Z_0 = \sqrt{\rho B}, \tag{2.7}$$

where symbols ρ and B stand for the mass density and the bulk modulus of the medium, respectively.

The role of the acoustic impedance in noise and vibration suppression devices can be easily demonstrated on the case of simple glass plate shown in Fig 2.2(a). Let us consider a sound transmission system, which consists of the glass plate fixed in a rigid frame at its edges. The plate creates an interface between two acoustic media of air. The interface is characterized by a specific acoustic impedance of the window Z_w. The sound source located underneath the glass plate generates an incident sound wave of the acoustic pressure p_i that strikes the glass plate. It makes the glass plate vibrate and a part of the sound wave is reflected and a part is transmitted with the values of the acoustic pressures p_r and p_t, respectively. Then, the specific acoustic impedance of the glass plate is defined as

$$Z_w = \frac{p_i + p_r - p_t}{v}, \tag{2.8}$$

which satisfies the equation of motion. Considering that the acoustic impedance is a frequency dependent property, one can work only with the amplitudes of the acoustic pressures, i.e. P_i, P_r, P_t and the amplitude of the vibrations, i.e. W. The frequency dependent specific acoustic impedance is expressed as follows, considering the simple assumption of a harmonic vibration response of the plate:

$$Z_w(\omega) = \frac{P_i(\omega) + P_r(\omega) - P_t(\omega)}{i\omega W(\omega)}, \tag{2.9}$$

where ω is the angular frequency, where $\omega = 2\pi f$, where f is the ordinary frequency in Hz. Assuming that by tuning the acoustic impedance of the planar structure at the interface of acoustic media can be changed the absorbing or reflecting capabilities of the interface, one can achieve devices such as perfectly absorbing surfaces or perfect sound shields.

In practice, the absorbing or reflecting capabilities of the structure are usually evaluated using the physical property called *acoustic transmission loss (TL)*. In noise suppression applications, the acoustic TL denotes the sound shielding efficiency of the interface structure. The value of acoustic TL is defined as a ratio, usually expressed in units of decibels, of the acoustic powers of the incident and transmitted acoustic waves, respectively:

$$\mathtt{TL} = 20 \log_{10} \left| \frac{p_i}{p_t} \right|, \tag{2.10}$$

Knowing the value of the specific acoustic impedance of the glass window Z_w, which is defined by Eq. (2.9), it is possible to derive the acoustic TL as follows: Let us use the simplified picture in Fig. 2.2(a) where the sound wave propagates through the glass shell from the acoustic medium below the shell to the acoustic medium above the glass shell along the z direction.

It is true that membrane velocity equals to (i) the particle velocity in the acoustic medium on the bottom side of the shell equals to the membrane velocity and (ii) the particle velocity in the acoustic medium in the upper side of the shell. This fact can be expressed by the following equation of motion:

$$-\frac{1}{i\omega\rho}\frac{\partial p}{\partial z} = Ve^{i\omega t}, \tag{2.11}$$

where the acoustic pressure p and the medium density ρ (i) at the bottom side of the shell are expressed as

$$p = P_i e^{i(\omega t - \frac{1}{c_0}z)} + P_r e^{i(\omega t + \frac{1}{c_0}z)}, \tag{2.12a}$$
$$\rho = \rho_0, \tag{2.12b}$$

where the symbol c_0 is the velocity of the sound in the acoustic medium below the shell, and (ii) at the upper side of the shell, the pressure is expressed as

$$p = P_t e^{i(\omega t - \frac{1}{c_1}z)}, \tag{2.13a}$$
$$\rho = \rho_1, \tag{2.13b}$$

where the symbol c_1 is the velocity of the sound in the acoustic medium above the shell. Using Eqs. (2.9), (2.11), (2.12a) and (2.13a), it is possible to obtain the following relations for the amplitudes of reflected acoustic pressure P_r, transmitted acoustic pressure P_t and the membrane velocity V:

$$P_r = -\frac{-P_i(Z_w + c_0\rho_0 - c_1\rho_1)}{Z_w + c_0\rho_0 + c_1\rho_1}, \tag{2.14}$$
$$P_t = \frac{2c_1 P_i \rho_1}{Z_w + c_0\rho_0 + c_1\rho_1}, \tag{2.15}$$
$$V = \frac{2P_i}{Z_w + c_0\rho_0 + c_1\rho_1}. \tag{2.16}$$

Then from Eqs. (2.6) and (2.11), it is possible to express the characteristic acoustic impedances Z_0 and Z_1, of the medium below and above the glass shell, respectively:

$$Z_0 = c_0\rho_0 \tag{2.17a}$$
$$Z_1 = c_1\rho_1. \tag{2.17b}$$

One can notice that it is possible to express the transmitted acoustic pressure amplitude, i.e. Eq. (2.15), in terms of characteristic acoustic impedance of the media and specific acoustic impedance of the shell:

$$P_t = \frac{2P_0 Z_1}{Z_0 + Z_1 + Z_w}, \tag{2.18}$$

And finally, when we substitute Eq. (2.18) into the definition formula for the acoustic TL, Eq. (2.10), assuming that the characteristic acoustic impedances of the media below and above the shell are equal, i.e. $Z_0 = Z_1 = Z_a$, where Z_a is the characteristic acoustic impedance of air, and $c_0 = c_1 = c$, where c is the sound velocity in air, and $\rho_0 = \rho_1 = \rho_0$, where ρ_0 is the density of air, we derive in the formula which was presented in [1]:

$$\mathtt{TL} = 20 \log_{10} \left| 1 + \frac{Z_w}{2Z_a} \right|, \tag{2.19}$$

where the acoustic TL is expressed only in terms of specific acoustic impedance of the glass shell/window Z_w.

Since the acoustic TL describes the sound shielding efficiency of the interface structure, it is clear that its value has to be increased in order to decrease the sound transmission through the interface. It can be seen from Eq. (2.19) that the acoustic TL will increase, when the specific acoustic impedance of the window increases. Fig. 2.2(b) presents a scheme of the noise suppression principle that follows from Eqs. (2.8) and (2.19), i.e., the values of specific acoustic impedance Z_w and acoustic TL increase with a decrease in the amplitude of the window vibration velocity v. The window is indicated to be thicker, so the amplitude of the vibrations W is smaller. As a result, the greater part of the incident sound wave energy is reflected than transmitted. In the most of applications, it is not possible or even desirable to make the planar structures, especially windows, thicker. One of the objective of the Thesis is to increase the acoustic TL without rising of the amount of material.

In order to optimize the system and to achieve maximum values of the acoustic TL, it is necessary to understand the dynamics and vibrational response of the glass plate. It is made using mathematical numerical simulations using the finite element method (FEM), which is presented further in next Chapters.

Chapter 3

Theoretical modelling of the acoustic impedance of a curved glass shell and the principles of active elasticity control method

In this Chapter, the possibilities in the active control of acoustic transmission loss (TL) of planar structures using the active elasticity control (AEC) method are analyzed. In the first step of the analysis, the most important parameters of the noise transmission system, which have an influence on the acoustic TL, are determined. In our particular case, an approximative analytical model of the vibration of curved glass shell is developed (see Sec. 3.1). Then, the specific acoustic impedance of the curved glass shell is calculated within the developed model. In the second step of the analysis, it is demonstrated that it is possible to control the elastic properties of the planar structure using an active piezoelectric layer attached to the planar structure (see Sec. 3.2). Finally, the basic theoretical aspects of the AEC method are explained (see Sec. 3.3).

3.1 Analytical estimation of the acoustic impedance of a curved glass shell

For simplicity, consider a rectangular-like glass shell of a constant thickness h and with the dimensions denoted by symbols a and b, which is shown in Fig. 3.1. Consider a curvilinear orthogonal coordinates x and y, that define the position on the curved surface of the shell. Consider that the

shell has constant radii of curvature along the x and y coordinates denoted by symbols R_x and R_y, respectively. It is convenient to introduce the symbols $\xi_x = 1/R_x$ and $\xi_y = 1/R_y$ for local curvatures of the shell along the x and y directions, respectively. Symbols u_x and u_y stand for tangential components of the displacement of the infinitesimal shell element with the volume $h\,dx\,dy$. The symbol w stands for the normal component of the displacement of the shell element. Using the fundamental equations presented in basic textbooks [10, 11, 12], one can derive to the equations of motion of the curved glass shell:

$$\begin{aligned} Yh\Bigg[\frac{1}{2(1-\nu^2)}\frac{\partial^2 u_x}{\partial x^2} + \frac{1}{2(1+\nu)}\frac{\partial^2 u_x}{\partial y^2} - \\ -\frac{1}{2(1-\nu)}\frac{\partial^2 u_y}{\partial x \partial y} - \frac{\xi_x + \nu\xi_y}{2\,(1-\nu^2)}\frac{\partial w}{\partial x}\Bigg] &= \varrho h \frac{\partial^2 u_x}{\partial t^2}, \qquad (3.1a) \\ Yh\Bigg[\frac{1}{2(1+\nu)}\frac{\partial^2 u_y}{\partial x^2} + \frac{1}{2(1-\nu^2)}\frac{\partial^2 u_y}{\partial y^2} - \\ -\frac{1}{2(1-\nu)}\frac{\partial^2 u_x}{\partial x \partial y} - \frac{\nu\xi_x + \xi_y}{2\,(1-\nu^2)}\frac{\partial w}{\partial y}\Bigg] &= \varrho h \frac{\partial^2 u_y}{\partial t^2}, \qquad (3.1b) \\ -G\Delta^2 w + \frac{Yh}{1-\nu^2}\Bigg[(\xi_x + \nu\xi_y)\frac{\partial u_x}{\partial x} + (\nu\xi_x + \xi_y)\frac{\partial u_y}{\partial y} - \\ -(\xi_x^2 + \xi_y^2 + 2\nu\xi_x\xi_y)w\Big] + \Delta p &= \varrho h \frac{\partial^2 w}{\partial t^2}, \qquad (3.1c) \end{aligned}$$

where

$$\Delta^2 w = \frac{\partial^4 w}{\partial x^4} + 2\frac{\partial^4 w}{\partial x^2 \partial y^2} + \frac{\partial^4 w}{\partial y^4} \qquad (3.2)$$

is the biharmonic operator. The symbols ϱ, Y, ν and G stand for the mass density, Young's modulus, Poisson's ratio and the bending stiffness coefficient of the material of the shell, respectively, the symbol Δp stands for the difference of the acoustic pressures at the opposite sides of the curved shell and represents the "driving force" of the system. It is seen that the first and second equations in Eqs. (3.1) represent the equations of motion for the tangential components u_x and u_y of the shell displacement. These are coupled with the normal component of the shell displacement w and the driving force Δp via the nonzero values of curvatures ξ_x and ξ_y. It can be shown that for relatively small numerical values of curvatures considered in this work, the values of all terms, which contain the tangential components u_x and u_y in Eq. (3.1c), are much smaller than the remaining terms with the normal component w of the displacement. Under this consideration, the system of Eqs. (3.1) can be further reduced down to a single partial differential equation in a form:

$$-G\Delta^2 w + \frac{Yh}{1-\nu^2}\left(\xi_x^2 + \xi_y^2 + 2\nu\xi_x\xi_y\right) w + \Delta p = \varrho h \frac{\partial^2 w}{\partial t^2}. \qquad (3.3)$$

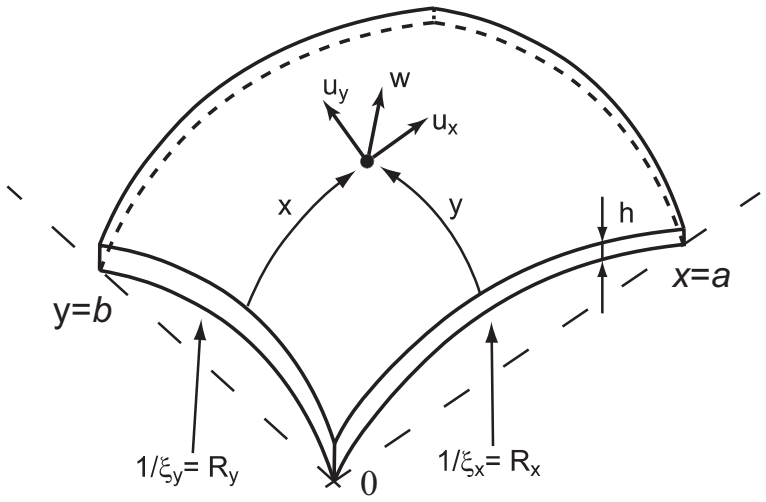

Figure 3.1: Geometry of the rectangular-like curved glass shell of constant thickness h. Symbols x and y stand for curvilinear orthogonal coordinates. The shell dimensions are denoted by symbols a and b. The shell has constant radii of curvatures along the x and y coordinates denoted by symbols $R_x = 1/\xi_x$ and $R_y = 1/\xi_y$. Symbols u_x and u_y stand for tangential components of the displacement of the infinitesimal shell element. The symbol w stands for the normal component of the displacement of the shell element.

When one considers a simple situation: (i) the shell is formed by a rectangular part of a spherical shell, i.e. $\xi_x = \xi_y = \xi$, (ii) the steady state, when the shell is driven by the pure tone of angular frequency ω, i.e. $\Delta p(t) = Pe^{i\omega t}$ and $w(x,\ y,\ t) = w(x,\ y)e^{i\omega t}$, and (iii) the boundary conditions of the simple supported shell, i.e. $w(0,\ y) = w(a,\ y) = w_{xx}(0,\ y) = w_{xx}(a,\ y) = 0$ and $w(x,\ 0) = w(x,\ b) = w_{yy}(x,\ 0) = w_{yy}(x,\ b) = 0$, the solution of the partial differential equation Eq. (3.3) can be easily found in the form of Fourier series:

$$w(x,y,t) = \sum_{n,m=1}^{\infty} \frac{16P(1-\nu)\sin\left[(2n-1)\pi x/a\right]}{(2n-1)(2m-1)\pi^2\{2Yh\xi^2 + (1-\nu)} \times \\ \times \frac{\sin\left[(2m-1)\pi y/b\right] e^{i\omega t}}{[G((2m-1)^2/b^2 + (2n-1)^2/a^2) - \rho h\omega^2]\}}. \tag{3.4}$$

Now, according to the Eq. (2.8), the effective value of the specific acoustic impedance z_w of the glass shell can be expressed in the following form:

$$Z_w(\omega) \approx \Delta p(0) \left[i\omega \sqrt{\frac{1}{ab}\int_a^0 dx \int_b^0 w(x,y,0)^2 dy} \right]^{-1}. \tag{3.5}$$

When we substitute the expression for the normal displacement of the spherical shell w from Eq. (3.4), one can arrive at the following formula for the effective specific acoustic impedance:

$$Z_w(\omega) \approx \approx \left\{ \sum_{n,m=1}^{\infty} \left[\frac{8i\omega a^2 b^2 (1-\nu)}{(2m-1)(2n-1)\pi^2 \left(G\,\zeta_{mn} + 2Yh\xi^2 - (1-\nu)\rho h\omega^2\right)} \right]^2 \right\}^{-1/2}, \tag{3.6}$$

where

$$\zeta_{mn} \;=\; \pi^4 (1-\nu)^2 (1+\nu) \left[(2m-1)^2/b^2 + (2n-1)^2/a^2 \right]^2 .$$

It is clear that Eq. (3.4) describes the displacement of the rectangular part of a spherical shell in a special situation without much practical interest. On the other hand, the presented analytical solution serves a possibility to trace the key features of the system that can be used for the suppression of the noise transmission.

First, it is seen that with an increase of the glass shell curvature ξ, the term $2Yh\xi^2$ in the denominator of Eq. (3.4) increases. This yields the decrease of the amplitude of the shell displacement and, therefore, the decrease of the normal velocity of vibrations. As a result, the value of the specific acoustic impedance of the glass shell Z_w increases with an increase in its curvature ξ as it can be seen in Eq. 3.6. The reason for this curvature effect is that the normal displacement of the curved shell is controlled by the in-plane stiffness, in addition to the bending flexural rigidity. Second, the specific acoustic impedance Z_w of the curved shell, i.e. $\xi > 0$, increases with an increase in the Young's modulus Y. Third, the value of Z_w of the plane plate, i.e. $\xi = 0$, increases with an increase in the bending stiffness coefficient G.

Now, it is clear, that the active control of the Young's modulus Y and the bending stiffness coefficient G would influence the vibrational response of the glass shell. Next section of the Thesis explains the basic principle how to do that by means of the attached piezoelectric layer to the planar structure.

3.2 Composite structure of the glass plate and piezoelectric element

Generally, bending piezoelectric devices consists of several piezoelectric and non-piezoelectric layers laminated together. Each layer has different material and geometric parameters. The motion of multilayer composite structures is described by equations of motion, see e.g. the Eqs. 3.1, where the

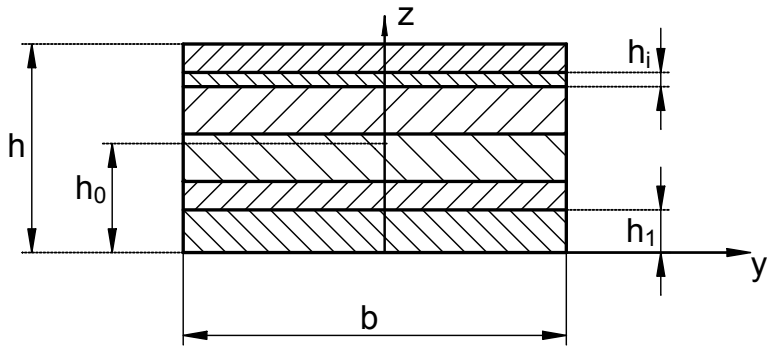

Figure 3.2: General multilayer structure with a rectangular cross-section placed in the system of coordinates. The structure has N layers of width b with different height h_i. The total thickness of the structure is denoted by the symbol h.

material and geometric parameters are replaced by their average values. These average values can be calculated by the integration of the partial parameters of the sublayers over the total cross-section [13].

Imagine a general multilayer structure with a rectangular cross-section area $S = bh$ according to Fig. 3.2. The structure has N layers of width b with different height h_i, cross-section area $S_i = bh_i$, density ρ_i and Young's modulus Y_i. The total thickness of the structure is denoted by the symbol h. The position of the neutral axis, which passes through the centroid of the cross-section, is denoted by h_0. Then, the average density ρ_{Eff}, average Young's modulus Y_{Eff} and the position of the neutral axis h_0 can be solved using following relations:

$$\rho_{\mathrm{Eff}} = \frac{1}{S}\int_S \rho dS = \frac{\sum_{i=1}^{N} \rho_i h_i}{h} \tag{3.7}$$

$$Y_{\mathrm{Eff}} = \frac{1}{S}\int_S Y dS = \frac{\sum_{i=1}^{N} Y_i h_i}{h} \tag{3.8}$$

$$h_0 = \frac{1}{Y_{\mathrm{Eff}} S}\int_S Y z dS = \frac{1}{2}\frac{Y_1 h_1^2 + \sum_{j=2}^{N} Y_j \left[\left(\sum_{k=1}^{j} h_k\right)^2 - \left(\sum_{k=1}^{j-1} h_k\right)^2\right]}{\sum_{i=1}^{N} Y_i h_i}. \tag{3.9}$$

The average bending stiffness G_{Eff} is calculated with respect to the position

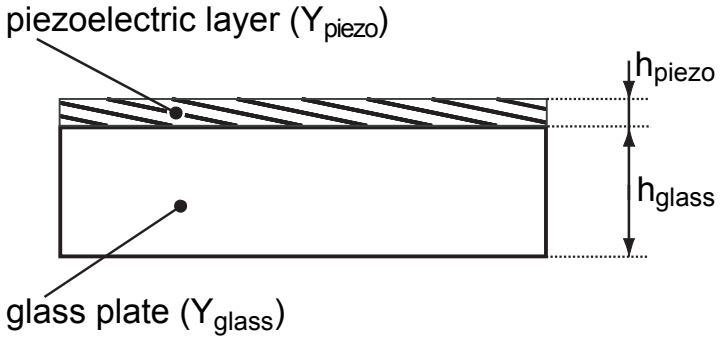

Figure 3.3: Cross-section of the layered composite structure, which consists of a glass plate of thickness h and Young's modulus Y_{glass} and an attached piezoelectric layer of thickness h_{piezo} and Young's modulus Y_{piezo}.

of the neutral axis as

$$G_{\text{Eff}} = \int_S Y z^2 dS = b \int_{-h_0}^{h-h_0} Y z^2 dS = \frac{1}{3} b \Bigg\{ Y_1 \left[(h_1 - h_0)^3 - (-h_0)^3 \right] + \\ + \sum_{j=2}^{N} Y_j \left[\left(\sum_{k=1}^{j} h_k - h_0 \right)^3 - \left(\sum_{k=1}^{j-1} h_k - h_0 \right)^3 \right] \Bigg\}. \tag{3.10}$$

Following the [13], let us consider a one of the typical layered configurations, simple bender with just two layers of different material and thicknesses, i.e. composite structure of the glass plate and the attached piezoelectric layer, with a cross-section shown in Fig. 3.3. The average (effective) Young's modulus of the whole structure Y_{Eff} is given by weighted average of the Young's moduli of the glass and the piezoelectric layer, according to the formula originated from Eq. (3.8):

$$Y_{\text{Eff}} = \frac{Y_{\text{glass}} h_{\text{glass}} + Y_{\text{piezo}} h_{\text{piezo}}}{h_{\text{glass}} + h_{\text{piezo}}}, \tag{3.11}$$

where the symbols Y_{glass} and Y_{piezo} stand for the Young's moduli of the glass and the piezoelectric material of the piezoelectric layer, respectively. The symbols h_{glass} and h_{piezo} stand for the thickness of the glass plate and the piezoelectric layer, respectively. Let us substitute the symbols Y and h for the symbols Y_{glass} and h_{glass}, for simplicity. Now, the average (effective) value of the bending stiffness coefficient G_{Eff} of the composite sandwich structure is given by the formula which originates from Eqs. (3.9) and

(3.10):

$$G_{\mathrm{Eff}} = \frac{Y^2 h^4 + Y_{\mathrm{piezo}}^2 h_{\mathrm{piezo}}^4 + 2 Y Y_{\mathrm{piezo}} h h_{\mathrm{piezo}} \left(2h^2 + 3 h h_{\mathrm{piezo}} + 2 h_{\mathrm{piezo}}^2\right)}{12\left(1-\nu^2\right)\left(Y h + Y_{\mathrm{piezo}} h_{\mathrm{piezo}}\right)}, \tag{3.12}$$

where ν is Poisson's ratio of the material.

It is clearly seen that if Young's modulus of the piezoelectric layer is increased, both effective values of the Young's modulus Y_{Eff} and the bending stiffness coefficient G_{Eff} of the composite sandwich structure are increased as well. And, it is seen from Eqs. (3.4) and (3.6) that with an increase of the effective Young's modulus of the piezoelectric layer, the specific acoustic impedance of the curved glass shell increases.

Now, it was demonstrated that by the piezoelectric layer attached to the planar structure it is possible to control the elastic properties of the whole system, so, the next section presents a principle and an implementation of a method for the active control of the Young's modulus of the piezoelectric material which can me attached as a control layer to the planar structure.

3.3 Active elasticity control of piezoelectric materials

The role of electromechanical interaction on the effective elastic properties can be amplified if an active shunt circuit is connected to the piezoelectric actuator. Such an approach was introduced by Date et al. [14] and is called the active elasticity control (AEC) method. When the method is adopted in vibration or noise transmission control applications, then thanks to the fact that the shunt circuit is by nature active, it belongs to the group of active piezoelectric shunt damping (APSD) methods.

The basic idea of the method is based on the superposition of direct and converse piezoelectric effects with Hooke's law. Let us explain the basic principle on the case when the piezoelectric element is exposed to the influence of incoming acoustic pressure as it could be seen in Fig. 3.5(a). That means, the external mechanical force is applied to the piezoelectric element. According to the Hooke's law the mechanical strain $\mathbf{S}$ is produced in the piezoelectric actuator and, the external force generates a charge Q on the electrodes due to the direct piezoelectric effect (see Fig. 3.5(b)). The generated charge is introduced to the electronic shunt circuit, which controls the electric voltage V on the electrodes of the piezoelectric element which is then deformed according to the inverse piezoelectric effect (see Fig. 3.5(c)). The total strain $\mathbf{S}$ of the piezoelectric actuator is then equal to the sum of both: the stress-induced strain (due to Hooke's law) and the voltage-induced strain (due to the converse piezoelectric effect). When the

voltage-induced strain cancels the stress-induced strain, the total strain of the piezoelectric actuator equals zero even if nonzero external stress is applied. This actually means that the effective Young's modulus of the piezoelectric actuator reaches infinity. This fact could be successfully used in the noise transmission control applications because when the acoustic wave strikes the element with infinite Young's modulus, the all acoustic energy is reflected from the surface and nothing is transmitted to the other side (Fig. 3.5(d)).

The shunt circuit, which implements the control of effective elastic properties of the piezoelectric actuator is the active negative capacitance (NC) shunt circuit. The key parameter, which controls the value of the effective Young's modulus of the piezoelectric actuator, is the capacitance of the circuit C. This fact can be derived, when the equations of state for the mechanical strain S_{ij} and the electric displacement D_i in the piezoelectric actuator, i.e. Eqs. (2.1d) are appended by the formula for the voltage $V = E_i h$ applied back to the electrodes of the piezoelectric element from the external capacitor of capacitance C:

$$V = -Q/C, \tag{3.13}$$

where $Q = D_i A$ is the charge generated on the electrodes of the piezoelectric actuator of electrodes area A.

Combining Eqs. (2.1d) and (3.13), it is possible to obtain the formula for the effective Young's modulus of the piezoelectric actuator shunted by the external capacitor [14]:

$$Y_{ijkl,\mathrm{shunted}} = \frac{T_{kl}}{S_{ij}} = \frac{1}{s^E_{ijkl}} \left(1 + \frac{k^2_{ijk}}{1 - k^2_{ijk} + \alpha} \right), \tag{3.14}$$

where k_{ijk} is the electromechanical coupling factor of the piezoelectric actuator ($0 < k_{ijk} < 1$), as introduced in Chap. 2, and $\alpha = C/C_S$ is the ratio of the shunt circuit capacitance C over the piezoelectric element static capacitance C_S at a constant mechanical stress T_{ij}, where $C_S = \epsilon^T_{ij} A/h_{piezo}$.

It can be seen from Eq. (3.14) that large values of the effective Young's modulus of the piezoelectric element can be achieved only when the capacitance of the external circuit C is negative. It follows from the Eq. (3.14) that, when

$$C = -(1 - k^2_{ijk}) C_S, \tag{3.15}$$

the effective Young's modulus reaches infinity.

This method allows to realize noise shielding and vibration isolation systems. Early applications of this system have been reported by Okubo et al. [15] and Kodama et al. [16]. The theoretical analysis of these systems was performed later by Mokrý [17, 18] and various applications

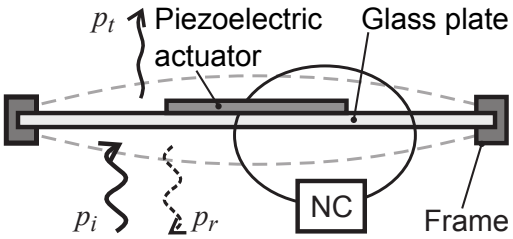

Figure 3.4: Scheme of the noise transmission suppression principle (cf. Fig. 2.2). The acoustic impedance of the plate is controlled using a piezoelectric actuator shunted by an active circuit. Vibration amplitude W normal to the glass surface is reduced by the action of the shunted piezoelectric actuator. In this way of damping, the greater part of the amplitude of the incident acoustic pressure wave is reflected from the plate than transmitted through the plate to the other side.

of an active elasticity control technique in the noise and vibration control devices were demonstrated by Fukada et al. [19, 20]. Imoto et al. [21] and Tahara [22] demonstrated the great potential of this method on a system for suppressing vibrations by 20 dB in the broad frequency range from 1 to 100 kHz. The low energy consumption was proved by Vaclavik and Mokry [23]. The noise shielding principle using the NC circuit was further theoretically analyzed by Sluka et al. [24]. Based on the theory introduced here and the already performed experiments by Okubo et al. and Kodama et al. and calculations by Mokry et al. and Sluka et al, the principle of AEC method could be profitably used when one needs to suppress the noise through the planar structure, e.g. the glass plate. Fig. 3.4 shows the scheme of the noise transmission suppression principle using a piezoelectric actuator shunted by an active circuit with negative capacitance. Following the Eqs. (3.4), (3.6), (3.11), (3.12) and (3.14), vibration amplitude W normal to the glass surface is reduced and subsequently the specific acoustic impedance is increased by the action of the shunted piezoelectric actuator. So, the greater part of the amplitude of the incident acoustic pressure wave is reflected from the plate than transmitted through the plate to the other side without the glass being thicker (cf. Fig. 2.2).

In the next Chapter, there will be introduced a piezoelectric actuator suitable for applications, which involves the potential problems of fragile vibrating structures such as glass plates. Using the finite element method simulations, it will be shown the effect of NC circuit on the average elastic properties of this piezoelectric actuator.

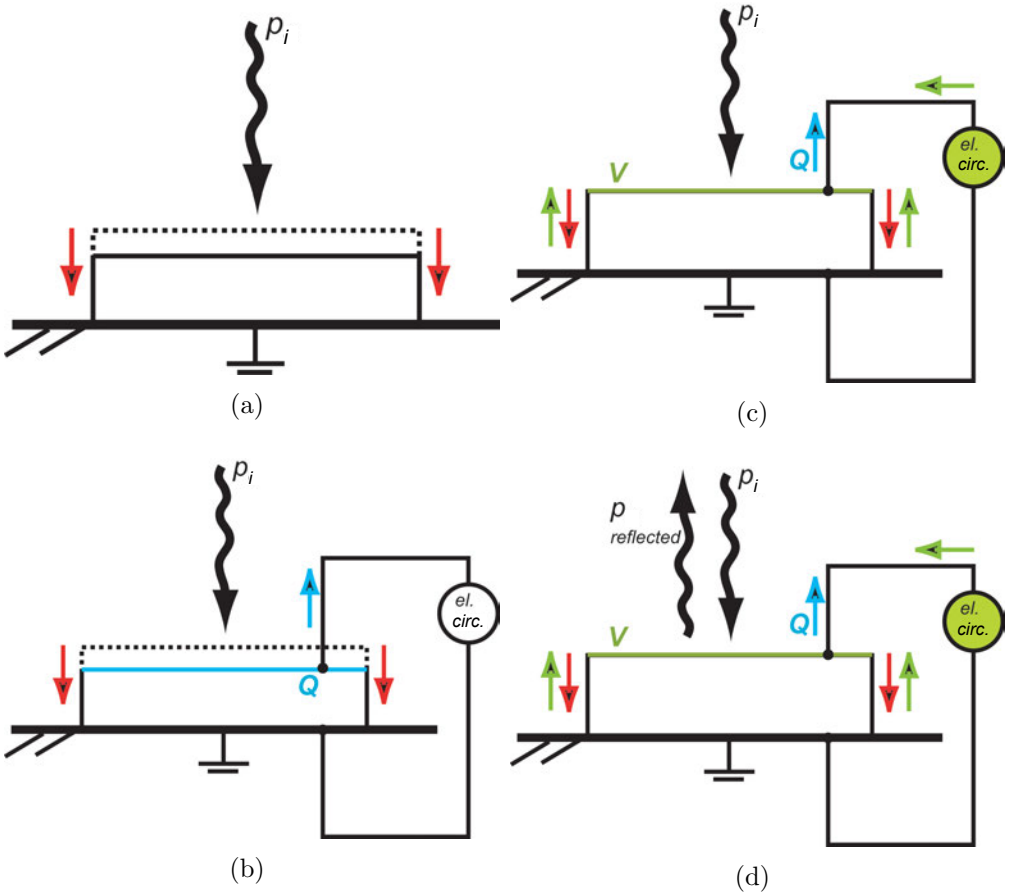

Figure 3.5: (a) The piezoelectric element is exposed to the influence of incoming acoustic pressure p_i. That means, the external mechanical force is applied to the piezoelectric element. It is deformed according to the Hooke's law (red); (b) The external force generates a charge Q on the piezoelectric element's electrodes due to the direct piezoelectric effect, the charge Q is introduced to the shunt electronic circuit (blue); (c) The electronic circuit controls the electric voltage V on the electrodes of the piezoelectric element which is deformed according to the inverse piezoelectric effect (green); (d) The total strain (the stress-induced strain (due to Hooke's law) and the voltage-induced strain (due to the converse piezoelectric effect)) of the piezoelectric actuator equals zero. This means that the effective Young's modulus of the piezoelectric actuator reaches infinity. Then, the all incoming acoustic energy is reflected from the surface and nothing is transmitted to the other side.

Chapter 4

Active elasticity control of macro fiber composite actuator

The flexible piezoelectric actuator, macro fiber composite (MFC) actuator, is introduced in this Chapter. Computation of its effective material properties and demonstration of tuning its effective elastic constants by means of a shunt electric circuit using FEM are presented here.

4.1 Introduction

Common PZT transducers are extremely brittle and they require extra attention during the handling and bonding procedures. They can easily crack, when they are exposed to large mechanical stresses or deformations. In addition, their conformability to curved surfaces is extremely poor [25]. Therefore, the concept of active piezoceramic composite transducers (PCT), which would contain PZT and some flexible adhesive to eliminate the aforementioned drawbacks has been explored. The new type of fiber reinforced PCT actuator, called macro fiber composite (MFC) actuator was developed at NASA Langley Research Center to eliminate many of the manufacturing and performance disadvantages [26]. Nowadays, both of these types of actuators are produced by Smart Materials Corp. [27].

MFC actuator is a layered planar actuation device that employs rectangular cross-section, unidirectional piezoceramic fibers from PZT-5A lead zirconate-titanate material embedded in an epoxy matrix which, first, inhibits crack propagation in a ceramic and, second, bonds the actuator together. This active fiber-reinforced layer is sandwiched between copper-clad polyimid film layers that have an etched IDE pattern. Nowadays, the MFC actuator retains the most advantageous features of the early PCT

actuators, namely, high strain energy density, directional actuation, conformability to all kind of surfaces and long durability. The fabrication process is uniform and repeatable so the actuator is financially accessible.

4.2 FEM model of the MFC actuator and the computation method

Composite materials, such as MFC, belong to the group of orthotropic materials. Therefore, the effective elastic properties of the MFC actuator can be represented by a matrix of elastic stiffness, introduced in Chap. 2, $\mathbf{c}_{\mathrm{MFC}}$ in a general form:

$$\mathbf{c}_{\mathrm{MFC}} = \begin{pmatrix} c_{11} & c_{12} & c_{13} & 0 & 0 & 0 \\ c_{12} & c_{22} & c_{13} & 0 & 0 & 0 \\ c_{13} & c_{13} & c_{33} & 0 & 0 & 0 \\ 0 & 0 & 0 & c_{44} & 0 & 0 \\ 0 & 0 & 0 & 0 & c_{44} & 0 \\ 0 & 0 & 0 & 0 & 0 & c_{66} \end{pmatrix}. \tag{4.1}$$

The inverse of the elastic stiffness matrix is the symmetric matrix of elastic compliances $\mathbf{s}_{\mathrm{MFC}}$ which could be defined in a form of Young's and shear moduli of the orthotropic MFC actuator:

$$\mathbf{s}_{\mathrm{MFC}} = \mathbf{c}_{\mathrm{MFC}}^{-1} = \begin{pmatrix} \frac{1}{Y_{11}} & \frac{-\nu_{21}}{Y_{22}} & \frac{-\nu_{31}}{Y_{33}} & 0 & 0 & 0 \\ \frac{-\nu_{12}}{Y_{11}} & \frac{1}{Y_{22}} & \frac{-\nu_{32}}{Y_{33}} & 0 & 0 & 0 \\ \frac{-\nu_{13}}{Y_{11}} & \frac{-\nu_{23}}{Y_{22}} & \frac{1}{Y_{33}} & 0 & 0 & 0 \\ 0 & 0 & 0 & \frac{1}{2G_{12}} & 0 & 0 \\ 0 & 0 & 0 & 0 & \frac{1}{2G_{23}} & 0 \\ 0 & 0 & 0 & 0 & 0 & \frac{1}{2G_{13}} \end{pmatrix}, \tag{4.2}$$

where Y_{11}, Y_{22}, Y_{33} are the Young's moduli, G_{12}, G_{23}, G_{13} are the shear moduli and ν_{12}, ν_{21}, ν_{13}, ν_{31}, ν_{23}, ν_{32} are the Poisson's ratios of the MFC actuator, whereas $\nu_{ij}/Y_{ii} = \nu_{ji}/Y_{jj}$.

The aforementioned elastic properties are considered as effective parameters of a large-scale/macroscopic structure. A common approach for numerical calculation of macroscopic properties of 3D piezoelectric fiber composites is to define a representative volume element (RVE) or a unit cell that captures the major features of the underlying microstructure. Fig. 4.1 shows the geometry of the RVE of the MFC actuator. It is placed in the coordinate system in such a way that the RVE center of mass is in the origin of the coordinate system and the PZT fibers are oriented along the x axis. The length of the cell, $l = 1000$ μm, contains two pitches of IDEs.

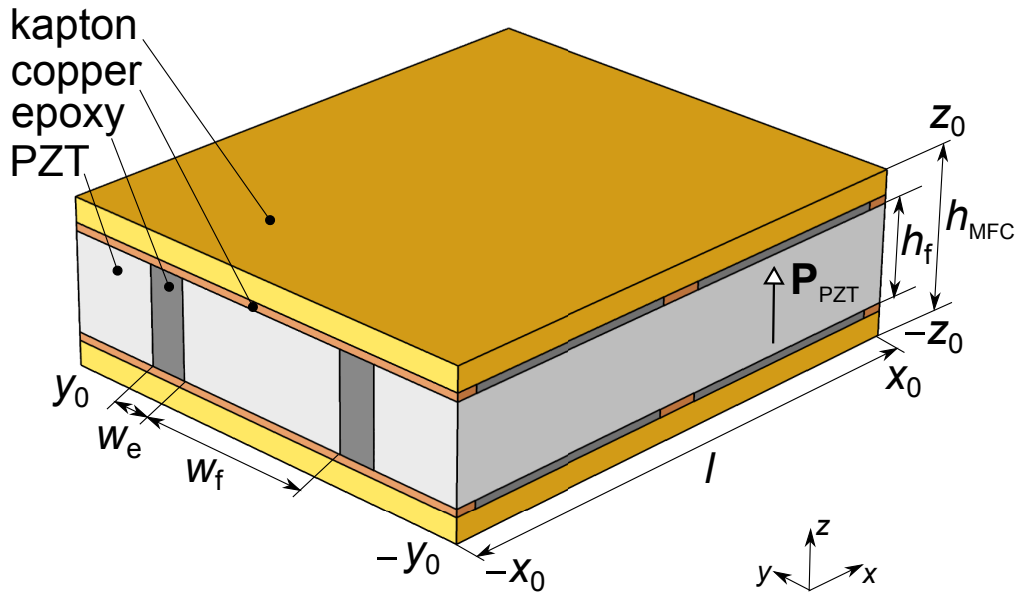

Figure 4.1: Geometry of the representative volume element model of the MFC actuator.

Width and thickness of the piezo-ceramic fiber are equal $w_f = 350$ μm and $h_f = 180$ μm, respectively. Fiber fill factor equals 83%, which, according to total dimensions of MFC actuators [27], gives the width of the epoxy gap between two PZT fibers, $w_e = 73$ μm. The total thickness of the MFC actuator is equal to $h_{\mathrm{MFC}} = 300$ μm. IDE copper electrodes are embedded in a kapton layer. The electrode finger and their width pitch are equal to 80 μm and 500 μm, respectively. In this Thesis, d_{31} effect MFC actuator is analyzed (it is called MFC of P2-type at Smart Material Corp. [27]). It means that piezoelectric fibers are polarized in the z axis direction and the actuator has an additional thin metal layer on each of the PZT fiber surface.

Fundamental equations that govern the electromechanical response of the MFC actuator are, first, the equation expressing the equilibrium of forces in the composite body, which is excited by external stimulus (i.e. mechanical force or electric field) of a harmonic time dependence with angular frequency ω:

$$-\rho\omega^2\mathbf{u} - \nabla\cdot\mathbf{T} = 0, \tag{4.3}$$

where ρ is the density of a material, $\mathbf{u}$ is the displacement vector distribution, and $\mathbf{T}$ is the mechanical stress tensor, and, second, Maxwell equation for the zero flow of electric displacement in the composite body:

$$\nabla\cdot\mathbf{D} = 0, \tag{4.4}$$

where $\mathbf{D}$ is electric displacement vector. In the case of static analyses, the angular frequency is equal to zero, i.e. $\omega = 0$.

In order to calculate the spatial distribution of electrostatic potential V and a deformation given by the displacement vector $\mathbf{u}$, it is necessary to introduce the complementary state quantities: the elastic strain tensor $\mathbf{S}$:

$$\mathbf{S} = \frac{1}{2}[(\nabla \mathbf{u})^T + \nabla \mathbf{u}] \tag{4.5}$$

and the electric field $\mathbf{E}$:

$$\mathbf{E} = -\nabla V. \tag{4.6}$$

In the isotropic non-piezoelectric material (i.e. epoxy, polyimide and copper), the relation between the above state quantities are given by constitutive equations that express the Hooke's law and the linear relationship between electric displacement and electric field,

$$\mathbf{S} = \frac{1}{Y}\mathbf{T} - \frac{\nu}{Y}(\mathrm{tr}(\mathbf{T})\,\mathbf{I} - \mathbf{T}), \tag{4.7}$$

$$\mathbf{D} = \epsilon_0 \epsilon_r\,(1 - j\eta)\,\mathbf{E}, \tag{4.8}$$

where Y and ν are Young's modulus and Poisson's ratio of an isotropic material, respectively. The symbol $\mathbf{I}$ stands for the second-order identity matrix. Symbols ϵ_0 and ϵ_r are the permittivity of a vacuum and dielectric constant of the material, respectively. Symbol η is the dielectric loss factor.

Material parameters of all isotropic composite constituents and piezoelectric PZT-5A adopted in the numerical model are listed in the Thesis.

In the piezoelectric material, the constitutive equations are given by the set of Eqs. 2.1, rewritten in the following matrix form:

$$\begin{aligned} \mathbf{D} &= [\epsilon^T]\,(\mathbf{I} - j\eta\mathbf{I})\,\mathbf{E} + [d]\mathbf{T}, \\ \mathbf{S} &= [d]\mathbf{E} + [s^E]\mathbf{T}, \end{aligned} \tag{4.9}$$

where $[s^E]$ are the elastic coefficients matrix for constant electric field, $[d]$ is the piezoelectric coefficients matrix, $[\epsilon^T]$ is the dielectric permittivity matrix at constant mechanical stress, and η is the dielectric loss factor.

In order to extent the validity of material parameters that were computed for the RVE of the MFC actuator to the full-size MFC actuator, several boundary conditions must be carefully specified.

In all the simulations, we consider a defined voltage on IDE electrodes of the MFC actuator. The bottom IDE electrode is grounded in all simulations. The top IDE electrode is considered grounded in the simulations of elastic parameters Y_{ii}, G_{ij}, and ν_{ij}. The applied testing voltage $V_0 = 100\,\mathrm{V}$ to the top IDE electrode is considered in the simulations of static capacitance per unit area of the MFC actuator and the piezoelectric coefficients d_{3i}.

The charge generated on the top IDE electrode is computed using a standard formula of electrostatics:

$$Q_0 = -\oint_{S_E} D_i n_i dS, \tag{4.10}$$

where n_i is the outer normal vector of the electrode.

It is assumed that the average mechanical and electrical properties of a RVE are equal to the average properties of the particular composite. The average stresses $\overline{T_{ij}}$ and strains $\overline{S_{ij}}$ in the RVE are calculated using formulas:

$$\overline{T_{ij}} = \frac{1}{V}\int_V T_{ij} dV, \tag{4.11a}$$

$$\overline{S_{ij}} = \frac{1}{V}\int_V S_{ij} dV, \tag{4.11b}$$

where V is the RVE volume. Then, the effective Young's moduli Y_{ii}, shear moduli G_{ij}, and Poisson ratios ν_{ij} can be expressed as:

$$Y_{ii} = \frac{\overline{T_{ii}}}{\overline{S_{ii}}}, \tag{4.12a}$$

$$G_{ij} = \frac{\overline{T_{ij}}}{2\overline{S_{ij}}}, \tag{4.12b}$$

$$\nu_{ij} = -\frac{\overline{S_{ii}}}{\overline{S_{jj}}}. \tag{4.12c}$$

In a similar way, our FEM model of the MFC actuator allows a simple method for the computation of the effective piezoelectric constants and static capacitance of the MFC actuator. In this case, a specific testing voltage V_0 is applied to the MFC actuator top electrodes and the average strain in the RVE is computed. Then the average piezoelectric moduli are calculated according to following formula:

$$d_{3ii} = \frac{\overline{S_{ii}}\, h_{\mathrm{MFC}}}{V_0}. \tag{4.13}$$

The static capacitance is given by the fundamental formula of electrostatics:

$$C_{S,0} = Q_0/V_0, \tag{4.14}$$

Using the developed FEM model and adopting the sets of Eqs. (4.11) and (4.12) and specifying the boundary conditions, effective elastic constants were computed and compared with data obtained using analytical

Material parameter	FEM model (this work)	Deraemaeker et al. [28]	Williams et al. [29]	Producer's datasheet [27]
Y_{11} (10^9 Pa)	32.58	27.27	29.4	30.34
Y_{22} (10^9 Pa)	15.33	14.76	15.2	15.86
Y_{33} (10^9 Pa)	9.37	-	-	-
G_{12} (10^9 Pa)	5.26	4.13	6.06	5.52
G_{23} (10^9 Pa)	2.47	-	-	-
G_{13} (10^9 Pa)	2.76	-	-	-
ν_{12} (1)	0.313	0.303	0.312	0.310
ν_{21} (1)	0.147	-	0.161	0.160
ν_{13} (1)	0.405	-	-	-
ν_{31} (1)	0.116	-	-	-
ν_{23} (1)	0.334	-	-	-
ν_{32} (1)	0.188	-	-	-

Table 4.1: Comparison of elastic parameters of the MFC (P2-type) actuator computed using FEM model (this work), analytical mixing rules, experimental measurements and MFC producer's datasheet values.

Material parameter	FEM model (this work)	Producer's datasheet [27]
S_{11}/V_0 (ppm/V)	-0.89	-1.1
S_{22}/V_0 (ppm/V)	-0.65	-
S_{33}/V_0 (ppm/V)	1.45	-
d_{31} (pm/V)	-267	-330
d_{32} (pm/V)	-196	-
d_{33} (pm/V)	425	-

Table 4.2: Comparison of free strain values S_{ii} and effective piezoelectric moduli d_{3ii} computed in this work with MFC's producer data sheet.

mixing rules and classical laminate theory by Deraemaeker [28], with results of experimental measurements by Williams at al. [29], and with values from the producer's datasheet [27]. The comparison is presented in Table 4.1. Results of computed piezoelectric coefficients are listed in Table 4.2 in comparison with the producer's datasheet [27]. The computed value of static capacitance is listed in Table 4.3, first, it is compared with the value calculated from producer's datasheet [27], and, second, with a rough estimate of the static capacitance per unit area of a capacitor, which is formed by in-parallel connection of two capacitors of the same thickness but with different dielectric constants. The two dielectrics are in this case PZT-5A and the epoxy material.

We can see an acceptable agreement of all the results computed in this work with the producer's values and with values obtained using another computational method.

Material parameter	FEM model (this work)	Analytical formula	Producer's datasheet [27]
$C_{S,0} = C'_S$ (10^{-5} F·m^{-2})	6.78	6.92	6.63
η_S (1)	0.010	-	-

Table 4.3: Results of the computed capacitance per unit area of the MFC (P2-type) actuator and the dielectric loss factor of the MFC (P2-type) actuator. Computed values are compared with rough estimate values using the formula for the capacitance of a capacitor with different dielectrics placed next to each other, and with the value obtained from the producer's datasheet.

Electromechanical coupling factor (1)	FEM model (This work)	Williams et al. [29]	Producer's datasheet [27]
k_{31}	0.339	0.357	0.362
k_{32}	0.177	0.213	0.218
k_{33}	0.286	-	-

Table 4.4: Comparison of computed values of the electromechanical coupling factors of the MFC (P2-type) actuator with a rough estimate calculated from the datasheet values.

4.3 Electromechanical interaction and the principle of AEC method adapted to MFC actuator elasticity control

As introduced before (see Chap. 3, Sec. 3.3), the electrical boundary conditions of piezoelectric actuators greatly affect their effective elastic properties. Using the FEM simulations electromechanical interaction of the MFC actuator with a NC shunt circuit could be analyzed in more complex way.

It is possible to implement the effect of the NC circuit into the FEM model as an electric circuit boundary condition on the top electrode while the bottom IDE electrode remains grounded.

The normalized values of Young moduli of the reference values presented in Table 4.1 are plotted as functions of the parameter α in Fig 4.2. It is seen that the values of the Young's moduli of MFC actuator are strongly influenced by the shunt circuit capacitance.

The curve of the normalized Young's moduli can be compared with theoretical formula Eq. 3.14. Using curves presented in Fig. 4.2, the values of effective electromechanical coupling factors can be obtained. Table 4.4

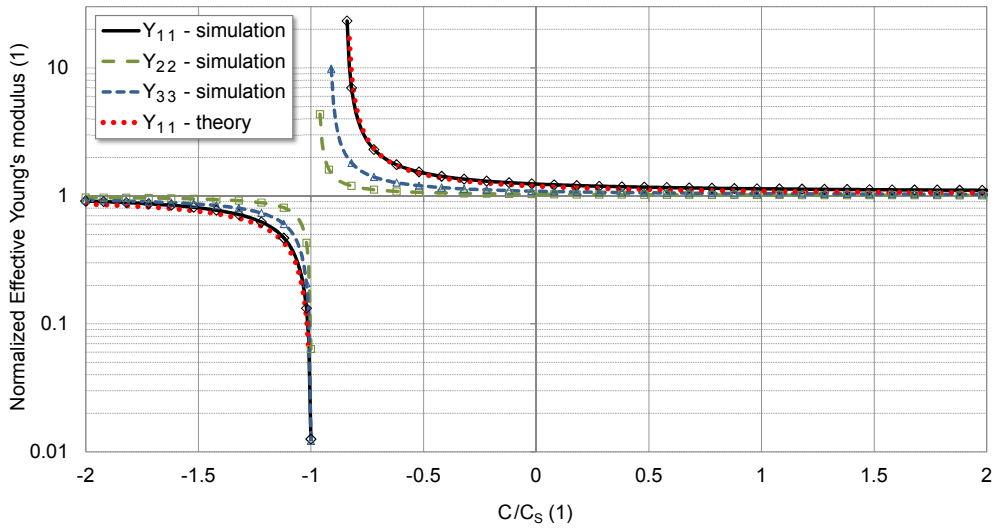

Figure 4.2: Normalized effective value of Young's moduli Y_{11}, Y_{22} and Y_{33} of MFC actuator dependent on the various adjustment of NC circuit.

presents the values of electromechanical coupling factors k_{3ii}, which were calculated using the least squares method.

The electrical scheme of a system, where the piezoelectric MFC actuator is shunted by a circuit that realizes negative values of capacitance, is shown in Fig. 4.3. The NC shunt circuit is realized as a negative impedance converter circuit (i.e. a one port circuit with an operational amplifier), where the reference impedance is realized as a capacitor C_0 connected in-series to the resistor R_0. The effective value of the shunt circuit capacitance is given by the formula:

$$C(\omega) = -\left(\frac{C_0}{1 + j\omega R_0 C_0}\right)\frac{R_2}{R_1}. \tag{4.15}$$

By proper adjustment of tunable resistors R_0 and R_1, the real and imaginary part of the shunt circuit effective capacitance can be adjusted in such a way that the condition given by Eq. (3.15) is satisfied and the effective Young's modulus of the MFC actuator is increased by several orders of magnitude.

In order to demonstrate the sensitivity of the NC circuit adjustment, it is convenient to rewrite the frequency dependence of the NC circuit into following parametrized form:

$$C(\omega) = -\frac{\xi\,(1 - k_{311}^2)\;C_S'\;(1 + \eta_S^2)}{1 + j\zeta(\omega/\omega_0)\eta_S}, \tag{4.16}$$

where $\xi = R_{1,\mathrm{opt}}/R_1$ and $\zeta = R_0/R_{0,\mathrm{opt}}$.

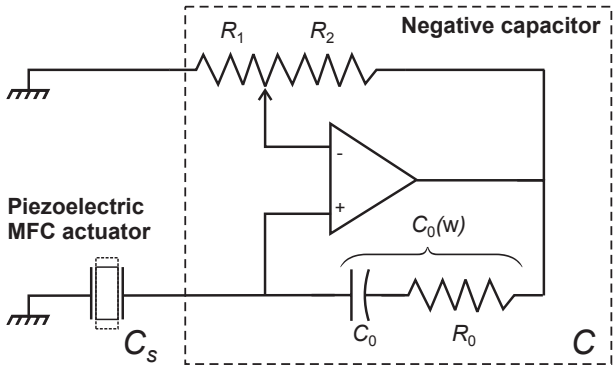

Figure 4.3: Electrical scheme of the piezoelectric MFC actuator shunted by the circuit that realizes negative values of effective capacitance.

To demonstrate that phenomenon, the sensitivity of the Young's modulus Y_{11} effective value to parameters ξ and ζ at the fixed critical frequency $f_0 = 850$ Hz was performed. The effective real part of Young's modulus Y_{11} is shown in Fig. 4.4. It is seen that the Young's modulus reaches the greatest values for $\zeta = 1.2$ and $\xi = 1.0081$.

Using the computed parameters ξ and ζ of the tuned NC circuit the frequency dependence of the effective orthotropic Young's modulus of the MFC actuator could be performed (Fig. 4.5), where real parts and the loss factors of the normalized effective Young's moduli are plotted for each Y_{11}, Y_{22} and Y_{33}. It can be seen that the theoretical dependence acceptably corresponds to computed data. Performed simulations show that it is possible to increase the effective Young's modulus Y_{11} by the factor of 1000 at the critical frequency (850 Hz).

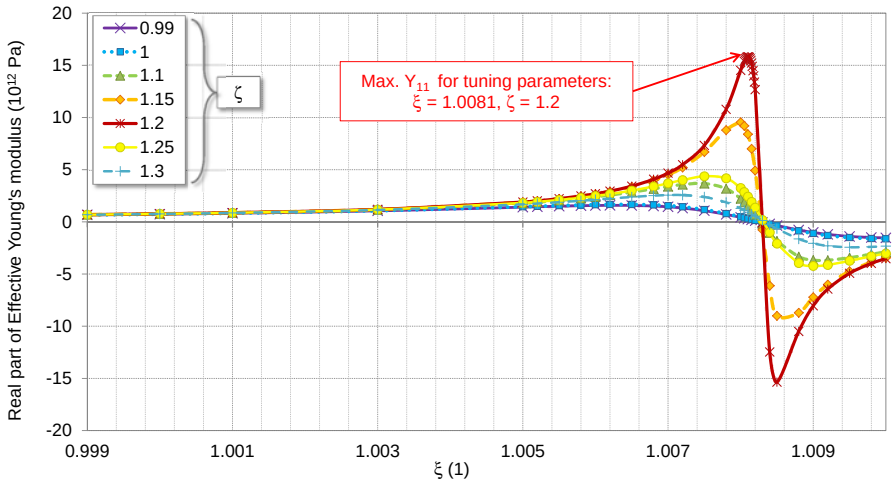

Figure 4.4: Tuning procedure of the capacity value of the NC circuit in order to maximize the real part of Young's modulus Y_{11}.

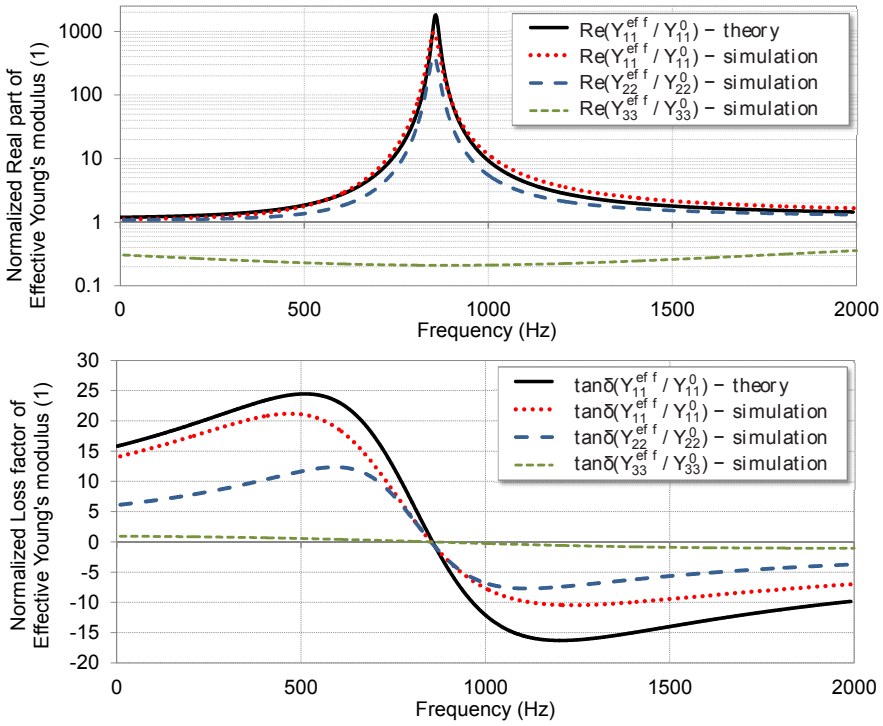

Figure 4.5: The real parts and loss factors of the normalized effective Young's moduli Y_{11} (thick solid), Y_{22} (thin solid), Y_{33} (dashed) and theoretical Y_{11} frequency dependence (dotted).

Chapter 5

Glass plate noise transmission suppression by means of distributed MFC actuators shunted by the negative capacitance circuit

Using the theoretical formula for the acoustic transmission loss calculated in Chap. 2, using the principles of the active elasticity control (AEC) method introduced in Chap. 3, and using the numerical results of the actively controlled Young's modulus of the macro fiber composite (MFC) actuator obtained in previous Chap. 4, the possibility of increasing the acoustic transmission loss of sound transmitted through planar or curved glass plates using attached piezoelectric MFC actuators shunted by the NC circuits is analyzed here using FEM and approximative experiments.

5.1 FEM model of the glass plate with attached MFC actuators

In order to analyze the noise transmission through the glass plate with attached MFC actuators it is convenient to develop a realistic FEM model which would be robust enough to see all the aspects of the vibrational response of the plate to the incoming pressure wave.

Figure 5.1 shows the geometry of the FEM model of a planar or curved glass plate of thickness h and dimensions a and b with 5 attached MFC actuators, placed in the system of coordinates. In the case of the curved geometry it is considered a glass plate, which could be fabricated by thermal

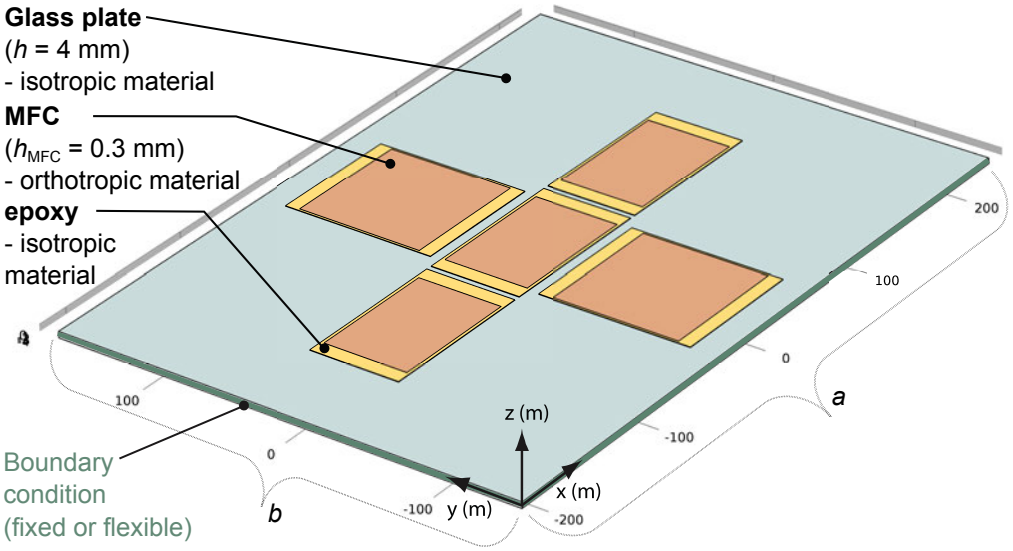

Figure 5.1: Geometry of the finite element method (FEM) model of a plane or curved glass plate of thickness with attached macro fiber composite (MFC) actuators.

bulging of the originally planar glass plate. The presented configuration of MFC actuators is selected in order to allow the suppression of majority of low-frequency vibrational modes.

The coupled analysis of the piezoelectric domain of the MFC actuator with the linear solid domain requires the same equations as it was introduced in the previous Chapter when the piezoelectric domain of the PZT fibers was coupled with an epoxy and polyimide material representing the linear elastic solid domain. Therefore, to check the governing equations, the reader is referred to see the Eqs. (4.3)-(4.9). Here, the piezoelectric domains the plates of the thickness h_{MFC} with some macroscopic values of elastic and piezoelectric coefficients representing the active part of MFC actuators and, the linear elastic domains are the glass plate with an epoxy embedding the active part of MFC actuators.

In the case of static analysis, a direct testing voltage is applied to the top electrode of the MFC actuator and the angular frequency is equal to zero, i.e. $\omega = 0$ and, in the case of dynamic analysis, a harmonic voltage of angular frequency $\omega = 2\pi f$ is applied to the top electrode of the MFC actuator, where the frequency f ranges from 10 Hz to 2 MHz. In both analyses, the bottom electrode is supposed to be grounded, i.e. the electric potential $V = 0$ V.

In the case of a coupled system of the flexible planar structure and the acoustic media, the effect of the flexible glass plate on the sound field below and above the plate as well as the effect of sound field on the flexible glass

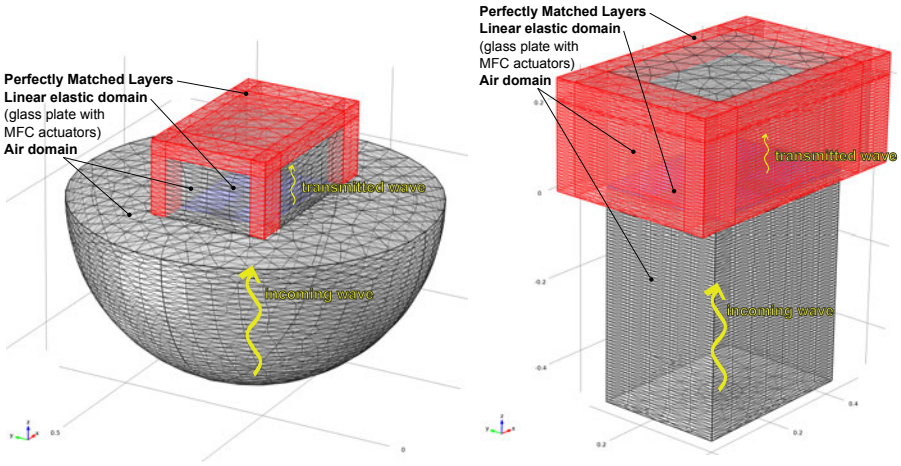

(a) (b)

Figure 5.2: Geometry and mesh of the considered linear elastic and air domains in the FEM model; (a) The incoming wave, which strikes the plate, goes from infinity; (b) The acoustic wave has a source in the bottom of the acoustic box.

plate must be considered together. First, the governing equation for each type of physics and second, the coupling variables should be introduced, respectively.

The vibrational response of the planar or curved glass plate and also the plates representing the MFC actuators is expressed by the displacement vector u_i is governed by the equations of motion in the form:

$$2\varrho\frac{\partial^2 u_i}{\partial t^2} - \nabla_j \left[c_{ijkl}\left(\nabla_k u_l + \nabla_l u_k\right)\right] = 0, \tag{5.1}$$

where ϱ is the mass density of glass, c_{ijkl} are the components of elastic stiffness tensor, and $\nabla_i = \partial/\partial x_i$ is the i-th component of the gradient operator. Since we are interested in the steady-state vibrational response of the plane/curved glass plate, we consider the harmonic time dependence of the displacement vector, i.e. $u_i(x,\, y,\, z,\, t) = u_i(x,\, y,\, z)\, e^{i\omega t}$, and the equations of motion Eq. (5.1) can be written in the form:

$$2\omega^2\varrho\, u_i + \nabla_j \left[c_{ijkl}\left(\nabla_k u_l + \nabla_l u_k\right)\right] = 0, \tag{5.2}$$

The effect of the shunt circuit can be introduced by means of frequency dependent values of the components of elastic stiffness tensor of the MFC actuator (see Chap. 4, Fig. 4.5).

Further, we consider that the glass plate with MFC actuators interacts with the acoustic field in the air above and below the plate. Fig. 5.2 sketches the acoustic air domains surrounding the linear elastic domain of

the glass plate. Two different cases are considered. First, the incoming wave, which strikes the plate, goes from infinity (Fig. 5.2(a)), second, the acoustic wave has a source in the bottom of the acoustic box which is supposed to simulate the real situation of the experiment performed to verify the simulations (Fig. 5.2(b)). In both analyses we consider a sound source that produces a plane incident wave below the glass plate:

$$p_i(z,t) = P_i\, e^{i(\omega t - kz)}, \tag{5.3}$$

where k is the wave number of the incident sound wave, which is oriented along the z-axis. The acoustic pressure p distribution in the air above and below the glass plate is governed by the following equation:

$$\frac{1}{\rho_0 c^2}\frac{\partial^2 p}{\partial t^2} + \nabla_i\left(-\frac{1}{\rho_0}\nabla_i p\right) = 0, \tag{5.4}$$

where ϱ_0 and c stand for the mass density and the sound speed in the air. Again, we are interested in the steady-state distribution of the acoustic pressure, i.e. $p(x,\, y,\, z,\, t) = p(x,\, y,\, z)\, e^{i\omega t}$, and the equation above reduces down to the form:

$$-\frac{\omega^2\, p}{\rho_0 c^2} + \nabla_i\left(-\frac{1}{\rho_0}\nabla_i p\right) = 0. \tag{5.5}$$

It should be noted that below the glass plate the acoustic pressure is given by the sum of the acoustic pressures of the incident and reflected sound waves, i.e. $p = p_i + p_r$. Above the glass plate, the acoustic pressure is equal to the acoustic pressure of the transmitted sound wave, i.e. $p = p_t$.

The boundary problem for partial differential equations given by Eqs. (5.2), (5.5) was solved using COMSOL Multiphysics software. The solution yields spatial distributions of the acoustic pressure p and the glass plate displacements u_i. Then, the specific acoustic impedance of the glass plate Z_w was estimated for every frequency ω of the incident sound wave using the following approximative formula:

$$Z_w(\omega) \approx \frac{\Delta P(\omega)}{i\omega W(\omega)}, \tag{5.6}$$

where ΔP is the amplitude of the acoustic pressure difference above and below the middle point of the glass plate, W is the amplitude of the normal displacement at the middle point of the glass plate. The acoustic TL was obtained using Eq. (2.19).

The governing equations should be appended by the numerical values of the material parameter and input variables which are clearly listed in the Thesis. Material parameters of the orthotropic MFC actuator are computed using the developed FEM model presented in previous Chapter. The

effective values are listed in Table 4.1. These parameters are suitable for the acoustic-structural analysis without the influence of the NC circuit. When the NC circuit is connected to the MFC actuators, the effect of the negative capacitance is introduced as a frequency dependent orthotropic Young's modulus according to the Fig. 4.5.

Numerical predictions of the FEM models should be compared with experimental data. The next Section presents a simple setup for obtaining experimental data.

5.2 Experimental setup for the FEM model verification

In this Section, a brief description of two different experimental setups that were used for the verification of FEM model predictions will be given.

First, the measurement of the surface displacement of the glass plate using the digital holographic interferometry (DHI) method and, second, the approximative acoustic measurements of the acoustic transmission loss.

The predictions of the numerical FEM simulations were verified by the digital holographic interferometry (DHI) measurements performed by the research group under the supervision of Dr. Vít Lédl, a specialist in optics and optical measurements.

DHI method is a possible way how to detect the distribution of surface vibration displacement of the planar structure. Fig. 5.3(a) shows a scheme of the setup for the measurement of the surface displacement distribution of the glass plate placed on the acoustic box. The laser beam is split into two beams by the polarizing beam splitter 1. Both beams are then spatially filtered and collimated. The object beam, the first beam, illuminates the sample – the glass plate – and the light scattered from its surface impinges on the beam splitter 2, where the reference and the object waves are recombined. The both waves interfere and a digital hologram is captured. The realization of the experimental setup of the glass plate surface displacement distribution measurement using the DHI method could be seen in Fig. 5.3(b). The glass plate is fixed in a wooden frame and placed on the acoustic box. Inside the acoustic box, the loudspeaker is used as a sound source. The acoustic waves generated by the loudspeaker strike the window plate making it vibrate. Using the DHI method, first, mode shapes of the glass plate are measured, and second, the static displacement of the glass plate with two attached MFC actuators connected to the direct voltage source is measured.

Second, Fig. 5.4 shows the experimental setup for the approximative measurements of the specific acoustic impedance. The glass plate

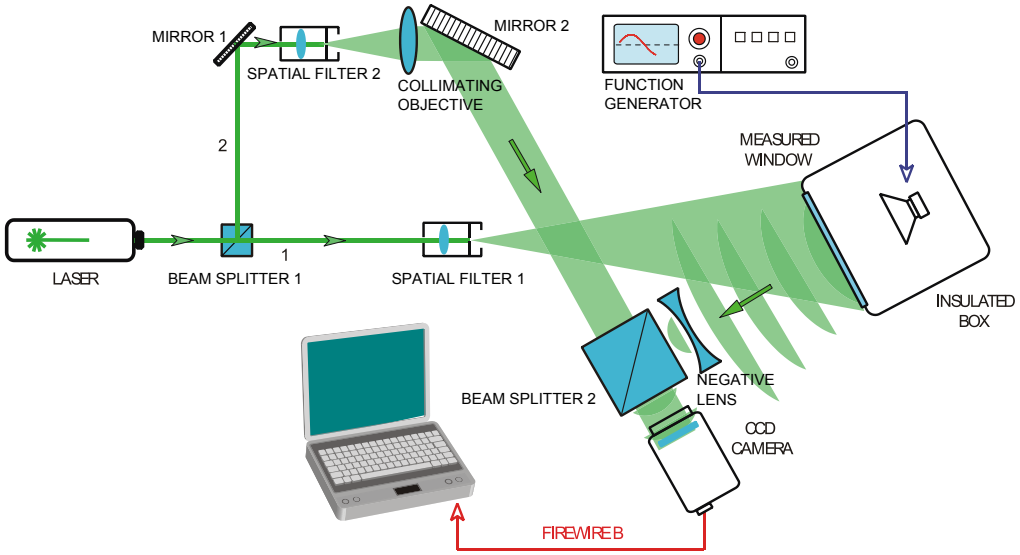

(a)

(b)

Figure 5.3: Digital holographic interferometry (DHI) measurement setup and realization; (a) Scheme of the glass plate surface displacement measurement using the DHI method.; (b) The photograph of a realization of the experimental setup of the glass plate surface displacement distribution measurement using the DHI method.

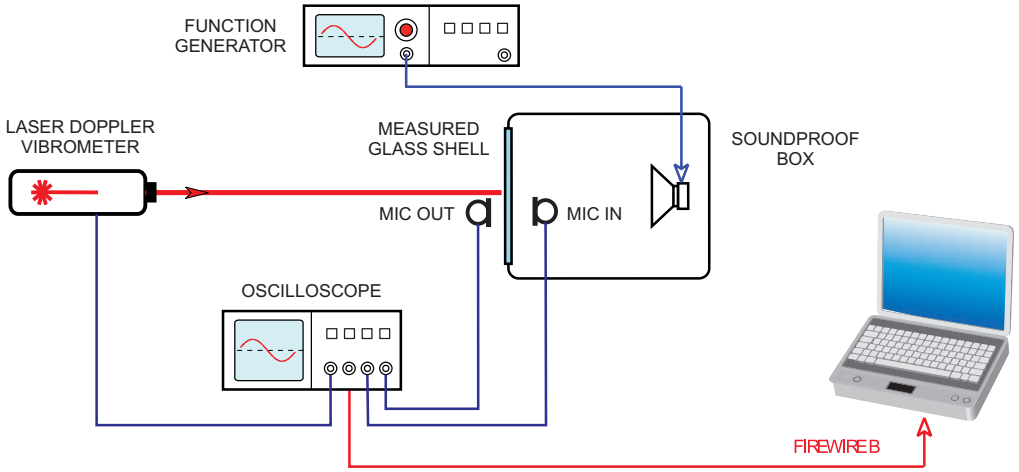

(a)

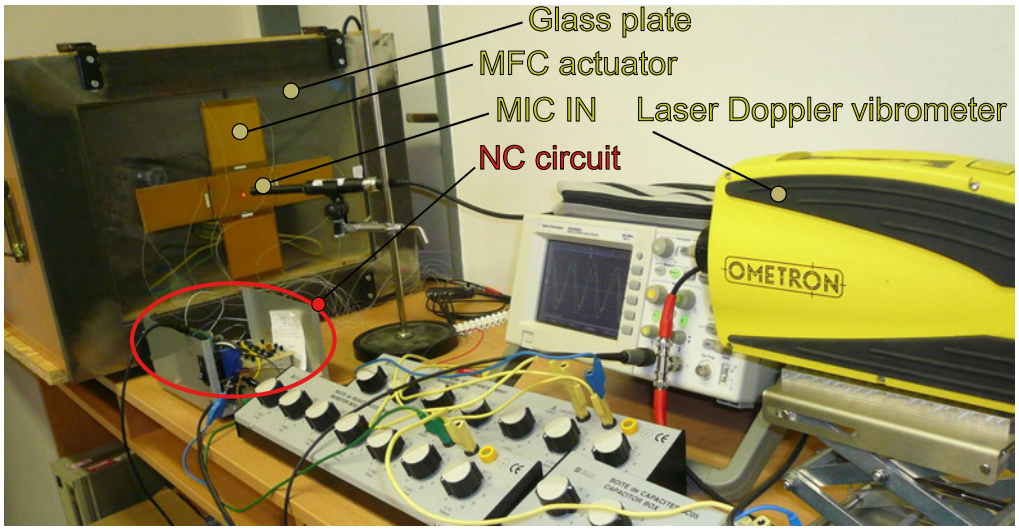

(b)

Figure 5.4: Experimental setup for the approximative measurements of the specific acoustic impedance; (a) Scheme of the measurement; (b) The photograph of a realization of the experimental setup of the approximative measurements of the specific acoustic impedance.

is clamped in a wooden or steel frame of the inner dimensions $a \times b$. This structure forms a lid of the soundproof box with a loudspeaker that produces the source of the incident sound wave. According to the scheme in Fig. 5.4(a), the microphone IN inside the box and the microphone OUT out of the wooden box measures the difference of acoustic pressures amplitudes ΔP at the opposite sides of the glass plate. They are placed approximately 1 cm above and below the middle point of the glass plate. Laser Doppler vibrometer measures the amplitude of the vibration velocity V of the glass plate middle point. The specific acoustic impedance Z_w is then approximated by the ratio $\Delta P/V$ and the value of the acoustic TL is estimated using Eq. (2.19). The realization of the experimental setup of the TL measurement could be seen in Fig. 5.4(b). The NC circuit is connected to the MFC actuators. Both cases, when the NC circuit is turned on and off, are measured. The acoustic transmission loss was measured for two cases, (i) when the MFC actuators are not connected to the NC circuit and (ii) when MFC actuators are shunted by the NC circuit. The next section presents the numerical results of our FEM model simulations and their comparison with the approximative experimental data.

5.3 Results of the FEM model simulations and the experimental verification

At first, results of FEM model simulations and DHI measurements of the surface displacement distribution will be presented. Second, the results of FEM model simulations and approximative measurements of the acoustic transmission loss frequency dependences will be shown appended by the graphical representations of the acoustic pressure distribution at the treated glass plate resonant mode.

Fig. 5.5 shows the static bending of the glass plate when the direct voltage of 300 V was applied on the electrodes of the MFC actuators. For this particular measurement a configuration setup with two MFC actuators was used. A photograph of the measured glass window with the MFC actuators clamped in a wooden frame could be seen in Fig. 5.5(a), the picture of the surface displacement of the glass plate captured by the DHI method is in Fig. 5.5(b) and last, for the result of FEM simulation of the glass plate displacement distribution stands Fig. 5.5(c). The white arrows locate the places where the MFC actuators were attached. It is evident that an acceptable agreement between the experimental values and the FEM simulations could be observed.

The dynamic response of the coupled system with attached MFC actuators on the harmonic voltage of the amplitude of 1 V could be seen in

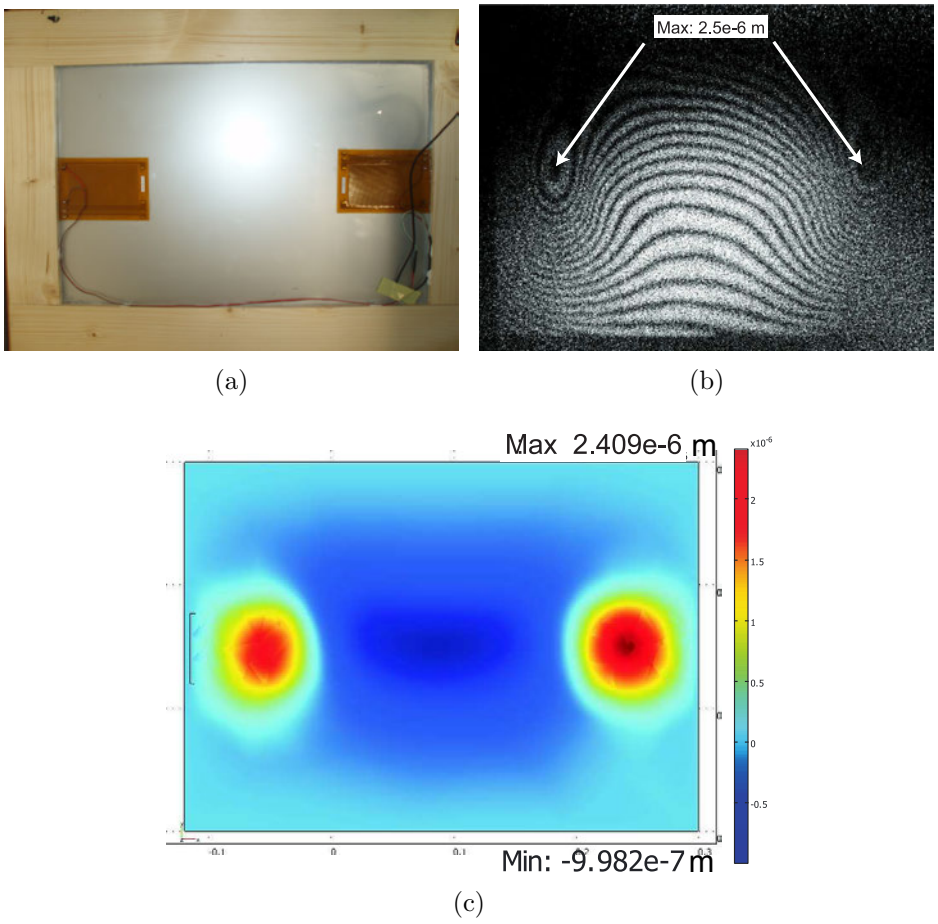

(a) (b)

(c)

Figure 5.5: Static bending of the glass plate due to the action of electrical voltage. DHI experiment with FEM model analysis comparison; (a) A photograph of the measured glass window with the MFC actuators clamped in a wooden frame; (b) Surface displacement distribution of the glass plate measured by the DHI method; (c) The result of FEM simulation of the glass plate displacement distribution.

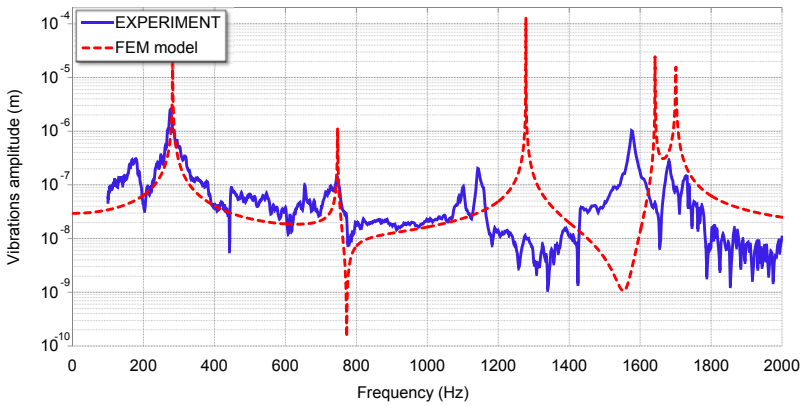

Figure 5.6: Dynamic response of the coupled system with attached MFC actuators on the harmonic voltage. The experiment data (blue solid) are compared with the FEM model ones (red dashed).

Fig. 5.6. The vibrations amplitude was measured in the middle point of the glass plate. The frequency range is limited from 10 Hz to 2 kHz. The experiment data (blue solid) are compared with the FEM model ones (red dashed). In the FEM model, the geometry with the steel frame which is put into the model as a additional mass is used. At the low frequency modes the acceptable agreement between the experiment and the FEM model is observed. On the other hand, at modes ensuing after 1 kHz value, the frequency dependence is shifted. One of the reason for this discrepancy could be the fact that in real situation of the experiment the steel frame is not ideally fixed. At higher frequencies the mass density and the Young's modulus of the glass are not the only dominant parameters which affect the resonant frequencies. It would be desirable to perform some additional FEM simulations to see how the boundary conditions of the frame affect the frequency dependence of the vibration amplitude of the glass plate, especially at the higher frequencies.

Figure 5.7 shows frequency dependence of the acoustic TL obtained from FEM model simulations considering the case of the acoustic wave, which strikes the glass plate incoming from infinity (Fig. 5.7(a)) and the case of the acoustic box with the sound source at the bottom (Fig. 5.7(b)). Four situations with different curvatures of the glass plate and the electrical conditions of the piezoelectric MFC actuators were considered: (i) Planar glass plate with opened MFC actuator (solid thick), (ii) bulged glass plate with opened MFC actuator (solid thin), (iii) planar glass plate with the MFC actuator shunted by NC circuit (dashed thick), and (iv) bulged glass plate with the MFC actuator shunted by NC circuit (dashed thin). The fixed boundary conditions at the edges of the glass plate are

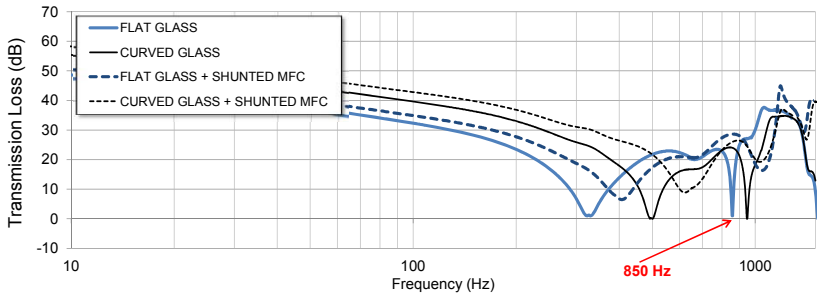

(a)

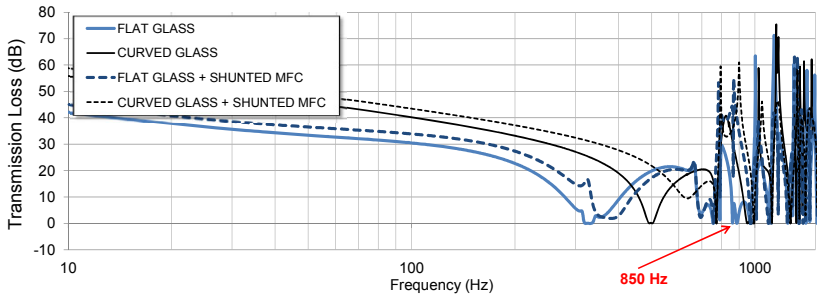

(b)

Figure 5.7: Frequency dependencies of the acoustic TL obtained from the FEM model simulations: Planar glass plate with opened MFC actuator (solid thick), bulged glass plate with opened MFC actuator (solid thin), planar glass plate with the MFC actuator shunted by NC circuit (dashed thick), and bulged glass plate with the MFC actuator shunted by NC circuit (dashed thin); (a) The acoustic wave which strikes the glass plate is incoming from infinity; (b) Acoustic box with the sound source at the bottom.

considered, i.e. $u_i = 0$. The bulged shape of the glass plate was approximated using the displacement function in the z-axis direction in the form $z_{\max} \sin(\pi x/a) \sin(\pi y/b)$, where $z_{\max} = 5$ mm.

Fig. 5.7 shows that an increase in the effective value of the Young's modulus of the MFC actuators has an appreciable effect on the frequency dependence of the acoustic TL through the glass plate. The numerical predictions of the FEM model indicate that it is possible to achieve the appreciable increase in the acoustic TL by about $10-25$ dB in the frequency range below 400 Hz due to the small increase in the curvature of the glass plate. In addition, it is noticeable that due to the effect of the NC circuit the the acoustic TL could be increased by about 25 dB at the second vibrational mode of the glass plate (850 Hz), what the NC circuit was tuned for. And finally, using the both effects, the curved shape of the glass plate and the NC circuit, the maximal increase of the acoustic TL can be

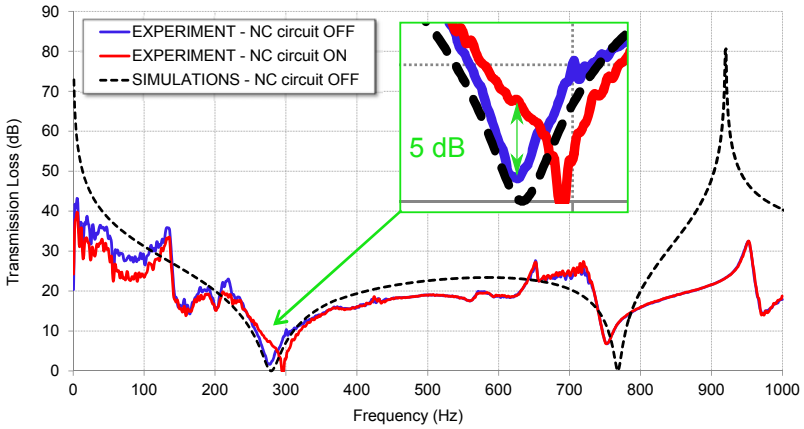

Figure 5.8: Results of the approximative measurements of the acoustic TL of the glass plate with attached MFC actuators which are opened (blue solid) and shunted by the NC circuit which is tuned at the frequency of the first vibrational mode of the glass plate (red solid).

achieved, particularly by about $10 - 30$ dB in the frequency range below 500 Hz and by about 25 dB at the second vibrational mode (850 Hz).

Finally, Fig. 5.8 shows the results of the approximative measurements of the acoustic TL of the glass plate with attached MFC actuators which are (i) opened, i.e. not connected to the NC circuit (blue solid), and (ii) shunted by the NC circuit which is tuned at the frequency of the first vibrational mode of the glass plate, i.e. the value of 276 Hz (red solid). It is possible to distinguish that at the frequency where the NC circuit was tuned the acoustic TL is increased by about 5 dB. The results without the NC circuit are compared with the FEM model simulations of the acoustic TL of the glass plate with the added steel frame (black dashed). The acceptable agreement of the experiment with the FEM model is observed.

The Chapter presents a promising approach for the suppression of the noise transmission through glass plates and shells using piezoelectric MFC actuators and negative capacitance circuits. As a result, the appreciable increase in the acoustic transmission loss through the glass plate composite can be observed.

A developed FEM model of the layered system of the planar structure with the piezoelectric layer can be used not only in structural-acoustic applications but also in structural-optic applications. The piezoelectric element attached to the planar structure can control its shape due to an applied electric voltage. In adaptive optics systems such deformable mirrors are the most commonly used wavefront correctors. A brief description of a deformable mirror that consists of a nickel reflective layer deposited on top of a thin PZT piezoelectric disk follows in the next Chapter.

Chapter 6

Application of the active shape control of the planar structure to adaptive optics

Deformable mirrors are the most commonly used wavefront correctors in adaptive optics systems. Nowadays, many applications of adaptive optics to astronomical telescopes, high power laser systems, and similar fast response optical devices require large diameter deformable mirrors with a fast response time and high actuator stroke. In this Chapter, an optimization of several geometric parameters of a deformable mirror that consists of a nickel reflective layer deposited on top of a thin piezoelectric PZT disk to get the maximum actuator stroke is presented using the FEM model of the layered structure.

Generally, the deformable mirror consists of a layered sandwich composite structure, where the reflective layer is bonded on a piezoelectric layer. The reflective layer is usually made of a conductive metallic material and forms an equipotential surface. On the opposite side of the piezoelectric layer a system of electrodes is deposited using conventional techniques such as lithographic sputtering. By applying a voltage to a particular electrode, the piezoelectric layer is deformed due to the inverse piezoelectric effect in the in-plane directions. This produces bending moments in the reflective layer of the particular segment of a deformable mirror and yield its out-of-plane deformation (see Fig. 6.1).

Geometry of the deformable mirror is presented in Figure 6.2. It consists of a double-layer sandwich composite structure in a shape of a disk of the radius R. In this study, the reflective layer of thickness h_{Ni} is made of nickel. The reflective nickel layer is bonded on a piezoelectric layer of thickness h_{PZT}. The reflective layer forms an equipotential at the bottom surface of the piezoelectric layer.

On the top surface of the piezoelectric layer, a system of honeycomb

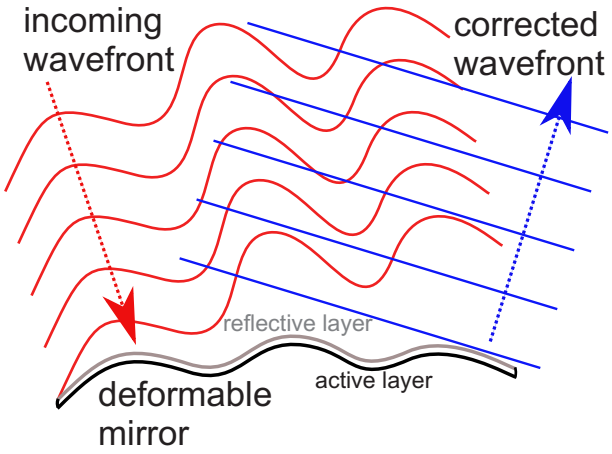

Figure 6.1: Principle of a deformable mirror. Incoming wavefront, which is distorted by atmospheric turbulence, is reflected from a deformable mirror, which corrects the shape of the wavefront to be planar again. In this study the deformable mirror is designed as a composite structure, where the reflective layer is bonded on the active piezoelectric layer.

golden electrodes is deposited using lithographic sputtering. It is considered that arbitrary external voltage can be applied at each particular electrode.

The equations which rule the analysis are the same as for the coupled analysis of the isotropic solid with the piezoelectrics, i.e. the Eqs. (4.3)-(4.9). Here, the piezoelectric domain is the thin PZT layer of the thickness h_{PZT} and, the isotropic linear solid domain is the reflective nickel layer of the thickness h_{Ni}.

As an example, Fig. 6.3 shows the graphical presentation of a result of the FEM numerical simulation of the deformable mirror. In the presented simulation, the off-centered honeycomb electrode is connected to the electric potential of 200 V, the remaining electrodes are short circuited. The surface boundary between the PZT and nickel layer is taken as a grounding electrode. Using the developed FEM model of the coupled structure of the two layers of isotropic with piezoelectric material, displacements of the deformable mirror are calculated and presented. Fig. 6.3(a) presents the 2D surface plot in the plane (xy) of the displacement of the mirror. Fig. 6.3(b) presents the plot along the line which goes along the diameter of the mirror through the all three honeycomb electrodes. Fig. 6.3(c) shows the 3D graphical interpretation of the displacement of the mirror which is shown using the iso-surfaces and slices.

In order to find the optimal ratio of the thicknesses of the nickel and PZT layers, a series of numerical FEM simulations has been performed. At the first step of each simulation, the geometry of the FEM model was mod-

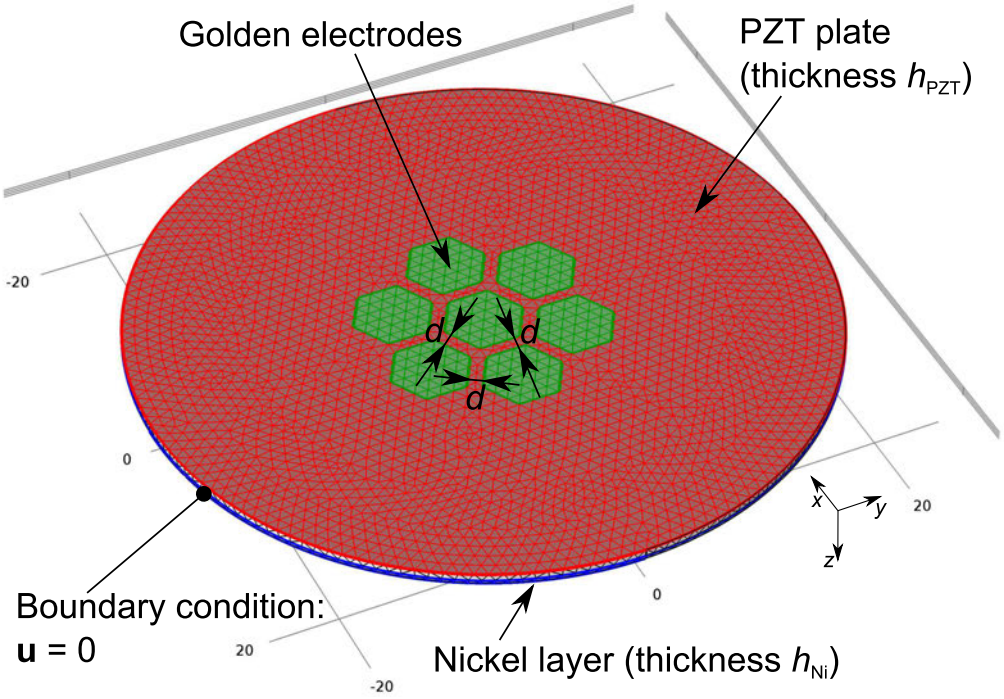

Figure 6.2: Geometry of the FEM model of the deformable mirror.

ified and the thicknesses of the nickel and PZT layers were set to particular values. In the second step, the displacement of the deformable mirror was calculated. In the third step, the value of the maximum deflection above the activated electrode was determined.

Figure 6.4 shows the result of the series of simulations, where the maximal values of the mirror deflection is plotted as a function of the nickel layer thickness h_{Ni} $(0.02 - 0.6$ mm). The parameter of each curve is the PZT layer thickness h_{PZT} $(0.2 - 0.8$ mm). All the combinations of the different thicknesses of the PZT and nickel layer were used for the FEM model. It can be seen that the thiner layers of both nickel and PZT are the larger displacement of the mirror can be achieved.

Brief description of the the obtained results indicates that the developed FEM model of the layered structure could be used across the research fields. In adaptive optics applications, it can provide an efficient and simple tool for the design of deformable mirrors with piezoelectric materials.

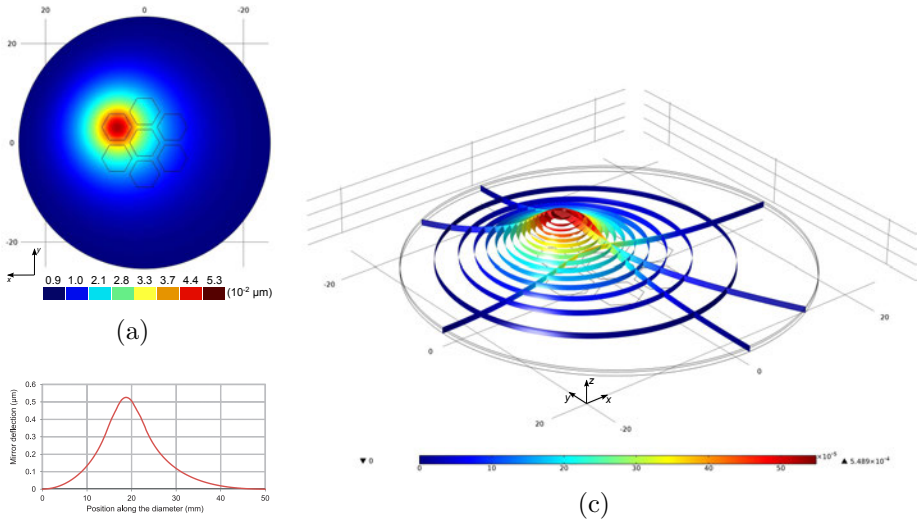

(a)

(b)

(c)

Figure 6.3: Graphical presentation of the deformable mirror displacement; (a) The 2D surface plot in the plane (xy) of the displacement of the mirror; (b) Plot along the line which goes along the diameter of the mirror through the all three honeycomb electrodes; (c) The 3D graphical interpretation of the displacement of the mirror, it is shown using the iso-surfaces and slices. The color legends mean the mechanical displacement value.

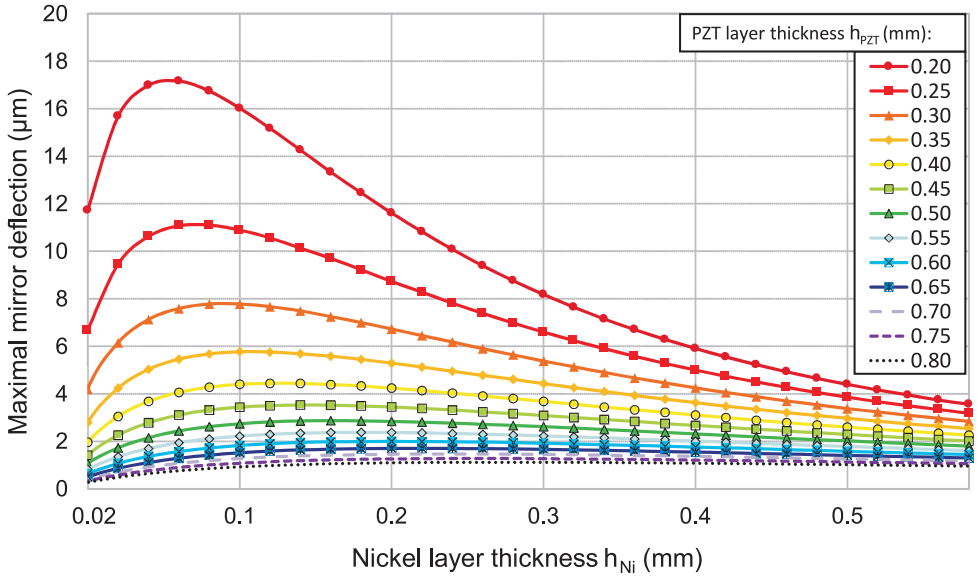

Figure 6.4: Dependences of the maximal values of the mirror deflection as a function of the nickel layer thickness. The parameter of each curve is the PZT layer thickness.

Chapter 7

Conclusions

The Thesis was focused on the study of possibilities to actively control the static and dynamic mechanical response of planar structures by means of attached piezoelectric actuators. It was shown that piezoelectric layered planar composite structures can offer an attractive approach for the reduction of amplitude of vibrations or for the electronic shape control. Therefore, these kind of controlled structures can provide an efficient tool with the use in applications of acoustics and adaptive optics.

In acoustics, the planar structure represents the interface between two acoustic media through, which the acoustic wave is propagating. It was shown that it is possible to control the amplitudes of the reflected and transmitted waves by controlling the amplitude of the planar structure vibration. A physical parameter, which expresses the sound shielding efficiency of the structure, is called the acoustic transmission loss. Its definition formula was presented in Chap. 2. The acoustic transmission loss was then expressed by means of the specific acoustic impedance Z of the interface between two acoustic media, i.e. of the planar structure.

In Chap. 3 the key parameters that control the acoustic transmission loss of the planar structure were determined using the analytical approximative model of the glass shell, which was considered of a plane or curved geometry. The basic conclusions from the theoretical model are the followings. With an increase of the glass shell curvature the amplitude of the shell displacement and subsequently the normal velocity of vibrations can be decreased. As a result, the values of the specific acoustic impedance Z_w and subsequently the acoustic transmission loss of the glass shell increase. Moreover, the specific acoustic impedance Z_w of the curved shell increases with an increase in the Young's modulus Y and the bending stiffness coefficient G of the glass shell and the value of Z_w of the plane plate, increases with an increase in the bending stiffness coefficient G of the plate.

Using the theoretical model of motion of the composite layered structure of the glass plate and the piezoelectric layer, it was shown that by

the piezoelectric layer attached to the planar structure it is possible to control the elastic properties of the whole system (see the Eqs. (3.11) and (3.12) for the effective Young's modulus and the bending stiffness coefficient, respectively, of the layered composite structure of the glass plate and piezoelectric actuator).

In Chap. 3, it was introduced the active elasticity control method that offers an alternative technique for the suppression of the noise transmission through piezoelectric structures or a technique for active suppression of vibrations of mechanical structures by attaching the piezoelectric elements to them. The idea is that by connecting a piezoelectric layer to the active shunt circuit with a negative capacitance the effective elastic properties of the piezoelectric element can be enhanced.

A suitable piezoelectric actuator, which can be simply attached to the various kind of surfaces (such as glass plate) and which is resistant to the cracking is the flexible macro fiber composite actuator. Its geometry, structure and fundamental properties were introduced in Chap. 4. In accord with the aforementioned approach and due to geometrical complexity of the macro fiber composite actuator, the numerical model of the macro fiber composite actuator based on the finite element method was developed to compute the effective material properties and to analyze the electromechanical interaction of the MFC actuator with the external electric negative capacitance circuit.

In Chap. 5, using the theoretical basics about the acoustic transmission loss stated in Chap. 2 and the findings about the active elasticity control method introduced in Chap. 3 and the results of the simulations of the actively controlled orthotropic Young's modulus of the macro fiber composite actuator obtained in Chap. 4, the possibility of increasing the acoustic transmission loss of sound transmitted through planar or curved glass plates using attached piezoelectric macro fiber composite actuators shunted by the negative capacitance circuits was analyzed using the finite element method numerical simulations and experimental measurements of the acoustic transmission loss.

First, the applicability and functionality of the macro fiber composite actuators attached to the glass plate was verified by the measurement of the static bending of the glass plate when the direct voltage was applied on the electrodes of the macro fiber composite actuators. The surface displacement of the glass plate captured by the digital holographic interferometry method is compared with the result of finite element simulation of the glass plate displacement distribution. An acceptable agreement between the experimental values and the simulations could be observed. Then, the dynamic response of the coupled system with attached macro fiber composite actuators on the harmonic voltage was performed. The experimental data are again compared with the finite element method model ones. At

low frequency modes the acceptable agreement between the experiment and the numerical model is observed.

In order to find the most effective way how to increase the acoustic transmission loss of the glass plate, the frequency dependencies of the acoustic transmission loss were computed using the finite element model simulations, which are based on the acoustic-structure interaction. The simulations compare the four situations with different curvatures of the glass plate and the electrical conditions of the piezoelectric macro fiber composite actuators: (i) Planar glass plate with opened macro fiber composite actuator, (ii) bulged glass plate with opened macro fiber composite actuator, (iii) planar glass plate with the macro fiber composite actuator shunted by negative capacitance circuit, and (iv) bulged glass plate with the macro fiber composite actuator shunted by negative capacitance circuit. It is shown that an increase in the effective value of the Young's modulus of the macro fiber composite actuators has an appreciable effect on the frequency dependence of the acoustic transmission loss through the glass plate.

According to the approximative acoustic measurement, the frequency dependencies of the acoustic transmission loss of the glass plate with attached macro fiber composite actuators which are (i) opened, i.e. not connected to the negative capacitance circuit, and (ii) shunted by the NC circuit which is tuned at the frequency of the first vibrational mode of the glass plate, i.e. the value of 276 Hz, show, that it is possible to distinguish that at the frequency where the negative capacitance circuit was tuned the acoustic transmission loss is increased by about 5 dB.

A developed finite element method model of the layered system of the planar structure with the piezoelectric layer can be used not only in structural-acoustic applications but also in structural-optic applications. The piezoelectric element attached to the planar structure can control its shape due to an applied electric voltage. In adaptive optics systems such deformable mirrors are the most commonly used wavefront correctors. A brief description of a deformable mirror that consists of a nickel reflective layer deposited on top of a thin PZT piezoelectric disk is presented in Chap. 6. A series of finite element method simulations were performed, in order to find optimal thickness ratio of the reflective and active layers to get the maximum out-of-plane deflections at minimum applied voltages to the piezoelectric structure. The linear regression of optimal values of the thicknesses of the nickel and PZT layers was determined.

The Thesis presents a promising approach for the suppression of the noise transmission through the plates and for the shape control of the plates using piezoelectric flexible composite piezoelectric actuators and active electronic circuits. The method starts from the vibrational analysis focusing on the effects of the elastic properties of the composite structures

with piezoelectric layers. Then, optimization of the parameters of the active electronic circuit has to be done to achieve the best performance of the actuator. The advantages of this method stem from its generality and simplicity offering an efficient tool for the control of the noise transmission through glass windows especially in the low-frequency range where the passive methods are ineffective and a simple and efficient tool for the shape control of large planar optical elements.

Bibliography

[1] Z. Maekawa, J. H. Rindel, and P. Lord, *Environmental and Architectural Acoustics*. CRC Press, 2 ed., Feb. 2011.

[2] K. Omae, T. Takebayashi, and H. Sakurai, "Occupational exposure limits based on biological monitoring: the japan society for occupational health," *International Archives of Occupational and Environmental Health*, vol. 72, pp. 271–273, July 1999.

[3] W. G. Cady, *Piezoelectricity: an introduction to the theory and applications of electromechanical phenomena in crystals*. University of California: Dover Publications, 1964.

[4] H. F. Tiersten, *Linear piezoelectric plate vibrations: elements of the linear theory of piezoelectricity and the vibrations of piezoelectric plates*. Plenum Press, 1969.

[5] IEEE, "ANSI/IEEE std 176-1987 standard on piezoelectricity," 1988. Standards.

[6] A. Arnau, *Piezoelectric transducers and applications*. New York: Springer, 2008.

[7] A. Safari and E. K. Akdogan, eds., *Piezoelectric and acoustic materials for transducer applications*. New York: Springer, 2008.

[8] A. Einstein, "Die grundlage der allgemeinen relativitätstheorie," *Annalen der Physik*, vol. 354, no. 7, pp. 769–822, 1916.

[9] K. Uchino, "Chapter 4 - 4.1 piezoelectric ceramics," in *Handbook of Advanced Ceramics*, pp. 107–159, Oxford: Academic Press, 2003.

[10] S. Timoshenko, *Theory of Plates and Shells*. McGraw-Hill Book Company, 1940.

[11] K. Graff, *Wave motion in elastic solids*. Dover Publication, 1991.

[12] W. Soedel, *Vibrations of Shells and Plates*. Marcel Dekker, 2004.

[13] S. W. Tsai, *Theory of Composites Design*. Think Composites, 1992.

[14] M. Date, M. Kutani, and S. Sakai, "Electrically controlled elasticity utilizing piezoelectric coupling," *Journal of Applied Physics*, vol. 87, no. 2, pp. 863–868, 2000.

[15] T. Okubo, H. Kodama, K. Kimura, K. Yamamoto, E. Fukada, and M. Date, "Sound-isolation and vibration-isolating efficiency piezoelectric materials connected to negative capacitance circuits," in *Proc. 17th International Congress on Acoustics*, pp. 301–306, 2001.

[16] H. Kodama, T. Okubo, M. Date, and E. Fukada, "Sound reflection and absorption by piezoelectric polymer films," in *Proc. Materials Research Society Symposium*, vol. 698, (506 Keystone Drive, Warrendale, PA 15088-7563 USA), pp. 43–52, Materials Research Society, 2002.

[17] P. Mokry, E. Fukada, and K. Yamamoto, "Noise shielding system utilizing a thin piezoelectric membrane and elasticity control," *Journal of Applied Physics*, vol. 94, no. 1, pp. 789–796, 2003.

[18] P. Mokry, E. Fukada, and K. Yamamoto, "Sound absorbing system as an application of the active elasticity control technique," *Journal of Applied Physics*, vol. 94, no. 11, pp. 7356–7362, 2003.

[19] E. Fukada, M. Date, K. Kimura, T. Okubo, H. Kodama, P. Mokry, and K. Yamamoto, "Sound isolation by piezoelectric polymer films connected to negative capacitance circuits," *IEEE Transactions on Dielectrics and Electrical Insulation*, vol. 11, pp. 328–333, APR 2004.

[20] E. Fukada, M. Date, and H. Kodama, "Recent trends on application of piezoactive polymers to acoustics," *Materials Technology*, vol. 19, pp. 83–90, JUN 2004.

[21] K. Imoto, M. Nishiura, K. Yamamoto, M. Date, E. Fukada, and Y. Tajitsu, "Elasticity control of piezoelectric lead zirconate titanate (pzt) materials using negative-capacitance circuits," *Japanese Journal of Applied Physics*, vol. 44, no. 9B, pp. 7019–7023, 2005.

[22] K. Tahara, H. Ueda, J. Takarada, K. Imoto, K. Yamamoto, M. Date, E. Fukada, and Y. Tajitsu, "Basic study of application for elasticity control of piezoelectric lead zirconate titanate materials using negative-capacitance circuits to sound shielding technology," *Japanese Journal of Applied Physics*, vol. 45, no. 9B, pp. 7422–7425, 2006.

[23] J. Václavík and P. Mokrý, "Measurement of mechanical and electrical energy flows in the semiactive piezoelectric shunt damping system," *Journal of Intelligent Material Systems and Structures*, vol. 23, pp. 527–533, 2012.

[24] T. Sluka, P. Mokry, and H. Lissek, "A theory of sound transmission through a clamped curved piezoelectric membrane connected to a negative capacitor," *International Journal of Solids and Structures*, vol. 47, no. 17, pp. 2260–2267, 2010.

[25] H. A. Sodano, G. Park, and D. J. Inman, "An investigation into the performance of macro-fiber composites for sensing and structural vibration applications," *Mechanical Systems and Signal Processing*, vol. 18, pp. 683–697, 2004.

[26] W. K. Wilkie, R. G. Bryant, J. W. High, R. L. Fox, R. F. Hellbaum, A. Jalink, B. D. Little, and P. H. Mirick, "Low-cost piezocomposite actuator for structural control applications," in *Society of Photo-Optical Instrumentation Engineers (SPIE) Conference Series* (J. H. Jacobs, ed.), vol. 3991, pp. 323–334, June 2000.

[27] "Smart material corp.." `http://www.smart-material.com`, 2000-2012.

[28] A. Deraemaeker, H. Nasser, A. Benjeddou, and A. Preumont, "Mixing rules for the piezoelectric properties of macro fiber composites," *Journal of Intelligent Material Systems and Structures*, vol. 20, pp. 1475–1482, Aug. 2009.

[29] R. B. Williams, D. J. Inman, M. R. Schultz, M. W. Hyer, and W. K. Wilkie, "Nonlinear tensile and shear behavior of macro fiber composite actuators," *Journal of Composite Materials*, vol. 38, no. 10, pp. 855–869, 2004.

Publications of the Author

[A.1] K. Nováková, P. Mokrý, J. Václavík, and V. Lédl, "Moderní trendy v semi-aktivním potlačování přenosu hluku skrz okenní tabuli pomocí piezoelektrických aktuátorů," *Silnice a železnice*, vol. 5, pp. IX–XIII, 2010.

- Journal Article

[A.2] K. Nováková, P. Mokrý, J. Václavík, and V. Lédl, "Analysis of noise transmission through the window glass plate and its control using the Macro Fiber Composite actuator," in *Proc. IEEE 19th International Symposium on Applications of Ferroelectrics*, Edinburgh, SCOTLAND, 2010, pp. 1–4.

- Presented at the 19th IEEE International Symposium on the Applications of Ferroelectrics (ISAF 2010), Edinburgh, SCOTLAND. (oral presentation)

[A.3] K. Nováková and P. Mokrý, "Numerical simulation of mechanical behavior of a Macro Fiber Composite piezoelectric actuator shunted by a negative capacitor," in *Proc. 10th International Workshop on Electronics, Control, Measurement and Signals (ECMS)*, Liberec, Česká republika, 2011, pp. 1–5.

- Presented at the 10th International Workshop on Electronics, Control, Measurement and Signals (ECMS 2011), Liberec, Česká republika. (oral presentation)

[A.4] K. Nováková and P. Mokrý, "Application of piezoelectric macro-fiber-composite actuators for the suppression of noise transmission through curved glass plates," in *Proc. 20th IEEE International Symposium on Applications of Ferroelectrics*, Vancouver, CANADA, 2011, pp. 1–5.

- Presented at the 20th IEEE International Symposium on the Applications of Ferroelectrics (ISAF 2011), Vancouver, CANADA. (oral presentation)

[A.5] K. Nováková and P. Mokrý, "Glass Plates Noise Transmission Suppression By Means of Distributed Piezoelectric Composite Actuators Shunted By an Active Circuitle," in *Proc. COMSOL Conference 2012 Milan*, Milan, ITALY, 2012.

- Presented at the COMSOL Conference 2012 Milan, ITALY. (poster)

[A.6] A. Kruchenko, K. Nováková and P. Mokrý, "Optimization of electrode geometry and piezoelectric layer thickness of a deformable mirror incoming corrected mirror," in *Proc. Optics and Measurement International Conference*, Liberec, Česká republika, 2012, pp. 69–73.

- Presented at the Optics and Measurement International Conference 2012, Liberec, Česká republika. (poster)

[A.7] K. Nováková, P. Mokrý, and J. Vaclavík, "Využití piezoelektrických kompozitních aktuátorů k potlačování přenášeného hluku skrz tenkostěnné plošné struktury," *Jemná mechanika a optika*, vol. 57, no. 11–12, pp. 300–307, Dec. 2012.

- Journal Article

[A.8] K. Nováková, P. Mokrý, and J. Vaclavík, "Application of piezoelectric macro-fiber-composite actuators to the suppression of noise transmission through curved glass plates," *IEEE Transactions on Ultrasonics, Ferroelectrics and Frequency Control*, vol. 59, no. 9, pp. 2004–2014, Sep. 2012.

- Journal Article

[A.9] A. Kruchenko, K. Nováková and P. Mokrý, "Optimization of electrode geometry and piezoelectric layer thickness of a deformable mirror incoming corrected mirror," in *EPJ Web of Conferences*, 2013, In Press.

- Journal Article In Press

[A.10] K. Nováková and P. Mokrý, "Numerical computation of effective material properties of Macro Fiber Composite actuator shunted by a negative capacitance circuit," *Composite Structures*, 2013, Submitted.

- Submitted Journal Article
- Under review